

MASTER'S THESIS 2020

Electro-thermal modeling of a battery cell set-up

ASHOK KUMAR VATSAVAI



Department of Electrical Power Engineering
Division of Electrical Engineering
CHALMERS UNIVERSITY OF TECHNOLOGY
Gothenburg, Sweden 2020

Electro-thermal modeling of a battery cell set-up
Ashok Vatsavai

© Ashok Vatsavai, 2020.

Supervisor: Zeyang Geng, Department of Electrical Power Engineering
Examiner: Torbjörn Thiringer, Department of Electrical Power Engineering

Master's Thesis 2020
Department of Electrical Power Engineering
Division of Electrical Engineering
Chalmers University of Technology
SE-412 96 Gothenburg
Telephone +46 31 772 1000

Electro-thermal modeling of a battery cell set-up
ASHOK VATSAVAI
Department of Electrical Engineering
Chalmers University of Technology

Abstract

Depletion of fossil fuels and stringent emission norms have boosted the growth of electric vehicles, and especially battery-powered electric vehicles (BEV). In comparison to the traditional fuel tank, managing battery pack energy in a BEV is quite challenging due to the temperature variations and therefore, there is a need for accurate testing methods. As most of the testing methods involve complex modelling, leading to an increased computational time, a simple testing method is necessary.

In this thesis work, a simplified model to predict the temperature distribution in a cell is presented. The measurements from the single cell, placed in a box under laboratory conditions, are taken as reference for the simplified model. First, a thermal model is created in COMSOL, considering all the dimensions and parameters from the single-cell box setup under laboratory conditions. Next, a more simplified Lumped Parameter Network (LPN) model is created, considering the thermal model as a reference. All the factors affecting the temperature distribution in an LPN model are investigated, and the results are presented. Also, for different scenarios, the thermal and LPN models are created, and the results are evaluated.

Finally, the temperature values from the thermal and LPN models are compared to the values from test setup under laboratory conditions. The resulting LPN model is in good agreement with both the thermal model and the test setup.

Keywords: cell charging, electro-thermal model, COMSOL model, LPN model, electric vehicle.

Acknowledgements

First of all, I would like to sincerely thank my examiner Torbjörn Thiringer for all his support and guidance throughout this thesis work, I would have never been able to complete my thesis work without his valuable insights and help. Also, I highly appreciate my supervisor Zeyang Geng, for her support and inputs, especially during the initial phase. I thank my family and friends for their support throughout my thesis work. Finally, I would like to give my gratitude to the ‘Division of Electric power Engineering, Chalmers University of Technology’ for allowing me to conduct this thesis work.

Ashok Kumar Vatsavai, Gothenburg, December 2020

Contents

1	Introduction	3
1.1	Problem Background	3
1.2	Previous Work	3
1.3	Purpose	4
1.4	Scope	4
1.5	Sustainable environment and Ethical Aspects	5
2	Theory	7
2.1	Plug-in Hybrid Electric Vehicles and Electric Vehicles	7
2.1.1	Plug-in Hybrid Electric Vehicles	7
2.1.2	Electric Vehicle	7
2.1.3	Importance of Quick Charging	8
2.2	Battery Properties	8
2.2.1	Thermal Properties	8
2.2.1.1	Conduction	8
2.2.1.2	Convection	8
2.3	Lithium-ion Batteries	9
2.3.1	Lithium-ion Battery Chemistry	9
2.3.2	Types of Battery Structures	10
2.3.3	Effect of Temperature on Lithium-ion Batteries	10
2.4	FEA Model	11
2.5	Lumped Parameter Model	12
2.6	Lumped Parameter Model vs FEA Model	12
2.6.1	COMSOL Model	13
2.6.2	LPN Model	14
2.7	Heat Spreading Angle	16
3	Base Comparisons	19
3.1	Styrofoam Blocks	19
3.1.1	Case-1	19
3.1.2	Case-2	20
3.1.3	Case-3	22
3.1.4	Case-4	23
3.1.5	Case-5	24
3.1.6	Conclusion:	26

4	Case Setup	27
4.1	Experiment setup of a cable attached to single cell box model	27
4.2	Cable	27
4.2.1	COMSOL Model	28
4.2.2	LPN Model	29
4.3	Single cell sealed box experiment setup and model	32
4.3.1	Box model with cell and aluminum blocks	33
4.3.1.1	COMSOL model	33
4.3.1.2	LPN Model	35
4.3.2	Box Model with Test Setup	37
4.3.2.1	COMSOL Model	37
4.3.2.2	LPN model	40
4.3.2.3	LPN model: Simple model	41
4.3.2.4	LPN model: Complex model	44
4.4	Box model with test setup and a cable attached	50
4.4.1	COMSOL Model	50
4.4.2	LPN Model	52
5	Results	55
5.1	Single cable: comparison of LPN VS COMSOL	55
5.1.1	Results from the COMSOL model	55
5.1.2	Results from the LPN model	56
5.2	Box model: comparison of LPN VS COMSOL	57
5.2.1	Results from the COMSOL model	57
5.2.2	Results from the LPN model	58
5.2.3	Comparison between COMSOL and LPN models	58
5.3	Single cell sealed box	60
5.3.1	Results from the COMSOL model	60
5.3.2	Results from the LPN model	61
5.3.3	Comparison of COMSOL and LPN models	62
5.4	Box model with a cable attached	63
5.4.1	Results from the COMSOL model	63
5.4.2	Results from the LPN model	63
5.4.3	Comparison of COMSOL and LPN models	64
5.5	Temperature variation at different heat rates	66
5.6	Temperature variation in the Box model with cable attached and assuming air flow	68
6	Conclusion	71
6.1	Conclusions	71
	Bibliography	I
A	Appendix 1	I
A.1	Others	I

List of Abbreviations

LPN	Lumped Parameter Network
EV	Electric Vehicle
BEV	Battery Electric Vehicle
HEV	Hybrid Electric Vehicle
PHEV	Plug-in Hybrid Electric Vehicle
ICE	Internal Combustion Engine
HT	Heat Transfer in Solids
LCO	Lithium Cobalt Oxide
EPDM	Ethylene Propylene Diene Monomer

Nomenclature

q_{cond}	Conductive heat transfer rate	W
k	Thermal conductivity	W/mK
dT/dx	Temperature gradient	K/m
A	Cross section area	m^2
q_{conv}	Convective heat transfer rate	W
h	Convection heat transfer coefficient	W/m^2K
Bi	Biot number	-
R_{therm}	Thermal resistance	K/W

1

Introduction

1.1 Problem Background

Depletion of fossil fuels along with stringent emission norms have boosted the research and growth of electrification in the field of transportation. However, this process of shifting from fossil fuel usage to electricity in the transportation industry has to overcome many challenges. One of the major challenges to overcome is managing a battery and its charging. This is primarily because of the battery pack energy limitation in comparison to a fuel tank storage. Therefore, to optimize the usage of an existing battery pack energy, many control and predictive models for battery pack testing have been developed.

On the other hand, the accuracy of these models in testing depends largely on the thermal variations in a single battery cell especially during charging. The estimation of these thermal variations in a single battery cell involves very accurate measurements and complex modelling, which further leads to an increased computational time during testing. Therefore, there is a need for a simplified test model, that makes this process easy and consumes significantly less time. Thus a lumped parameter network (LPN) model, which considers resistance and capacitance in an element to determine the temperature variations is proposed.

The LPN model is based on a physical model that is designed to investigate the effect of temperature on a single battery cell during quick charging. The physical model is designed using a tool by considering the measurement data of the exact practical model. This model is the reference for a lumped parameter network model and the variations in the physical model can be further evaluated to quantify the considerations in a set of stacked cells.

Thus a better estimation of battery thermal variations during charging with less computational time and complexity will be presented.

1.2 Previous Work

For charging a battery pack efficiently and quickly, the estimation of battery performance for different temperature variations is critical. Though there are a lot of studies disclosing such estimations, the models developed for these estimations are

not accurate. The primary reason for such an inaccuracy is the lack of precise loss estimation models for a single battery cell at different temperatures. Also, the computational time taken for these models, which are very detailed due to the materials and components used in the actual case, is usually very high. In addition to these, measuring accuracy for modeling and conditions considered for these measurements may also effect the model accuracy.

Thus, models that avoid such a high computational time and at the same instance provide a reasonable loss estimation of a single cell with predictable variations in the measurement values are necessary.

1.3 Purpose

The purpose of this thesis is to perform thermal modelling of a single battery cell during quick charging and simplify the thermal model using a lumped parameter network model of the same battery cell.

The advantage of this LPN model is its simplicity and the time taken for computation. The comparison between the physical model and LPN model will help in providing a better estimation of parameter variations and limitations.

1.4 Scope

An LPN model and a physical model to understand temperature variations in a single cell will be designed. The LPN model will be designed considering the physical model, that is designed from the measurements taken from a physical setup. However, the following limitations shall be considered while performing this study.

The physical model built in COMSOL will not be an exact model, as there can still be heat leaking from the physical model in the form of air gaps. Also in the COMSOL model, the surface of different components is considered as smooth and small variations in the surfaces will be neglected. However, all of the important parameter considerations to replicate the existing practical model will be incorporated in the COMSOL model.

The LPN model will be based on the physical model. However, complex modelling is performed only in the case of specific components. Therefore, there may be variations between the LPN model and the actual model. And the variations due to the neglected parameters if any in the COMSOL model are taken into account while documenting.

1.5 Sustainable environment and Ethical Aspects

The primary problems associated with EVs are fuel capacity and travelling range, unlike vehicles depending on gasoline, the charging time in the case of EVs is more. As battery performance and efficiency are the key factors in optimizing energy management in EVs, understanding the thermal behavior in battery cells is quite useful in estimating battery performance. Further, accurate energy management in EVs will not only enhance the reliability on EVs from a user perspective but also will lead to more people preferring EVs over ICE based vehicles helping environment sustainability.

The current study of electro-thermal modelling provides a quick indication of thermal variations within a cell, thus reducing the processing time required to predict the temperature variations. Though the complex predictive models used are slightly more accurate, they take longer processing time and power, which would delay the battery performance optimization process in real-life scenarios. Further, the simplified model presented in the current study can be modified and adjusted easily for different use cases. Most of the work carried out in the current study is computer-based and this approach reduces the resources required in comparison to a lot of experimental testing. Thus this method is will be preferable from an environment perspective.

2

Theory

In this chapter the background theory of this thesis work will be described. The explanation will start with the thesis title and continues further with the description of key components, their properties and differences in detail.

2.1 Plug-in Hybrid Electric Vehicles and Electric Vehicles

2.1.1 Plug-in Hybrid Electric Vehicles

A hybrid electric vehicle contains a hybrid power train which is the combination of an internal combustion engine as well as an electric machine. This combination allows such vehicles to use the operating efficiency of an electric machine at low speeds as well as for recuperating the braking energy by utilizing the same machine as a generator. And at high speed, the combustion engine is very efficient and can be operated as a conventional vehicle. These vehicles are also equipped with a battery pack in addition to the fuel tank to provide the power required for the electric machine as well as to store the recuperated energy from braking. Additionally, this hybridization of a power train gives the feasibility of downsizing the combustion engine, which can be compensated further by the electric machine if higher speeds are required. Thus, reducing carbon emissions significantly.

Plug-in hybrid electric vehicle's batteries are supplied with an external power source in addition to the conventional on-board sources as in hybrid electric vehicles.

2.1.2 Electric Vehicle

An electric vehicle contains an electric machine as the main and the only source of propulsion. Same as in HEVs, a battery pack is provided to power the electric machine as well as to store the recuperated energy. The battery is usually powered by an external plug-in power source through a cable and the charging time depends on the power source as well as on the battery pack intake capacity. The absence of a combustion engine thereby eliminates carbon emissions and makes these vehicles highly recommended for pollution-free transportation.

2.1.3 Importance of Quick Charging

In any vehicle, the range and performance are very important, and these are directly or indirectly linked to the vehicles fuel gauge and even EV, PHEVs are no exception to this. However, in EVs and PHEVs the battery size and the amount of power it delivers decides the range and performance. In the case of bigger batteries, the charging time plays a significant role as this feature is the key differentiator among conventional vehicles, EVs and PHEVs. Thus quick charging techniques are gaining prominence and are widely explored.

2.2 Battery Properties

The properties of a battery which we will be focusing on, in this thesis will be explained in this section.

2.2.1 Thermal Properties

2.2.1.1 Conduction

When two bodies that are at different temperatures are in physical contact with each other, heat transfers from the hot body to the cold body takes place. This process of heat transfer takes place primarily due to direct molecular collision and continues until both the bodies are at the same temperature [2].

The process of heat transfer can be quantified in terms of appropriate rate equations and the rate equation with a temperature distribution $T(x)$ is given as

$$q_{cond} = kA \frac{dT}{dx} \quad (2.1)$$

where q_{cond} is the conductive heat transfer rate, k is the thermal conductivity, dT is the temperature difference and dx is the length and A is the cross-section area across which the conduction phenomenon takes place [2, 3].

2.2.1.2 Convection

The process of heat transfer resulting from the thermal expansion of gases or liquids is called convection. This process of heat transfer is associated with liquids and gases, unlike conduction, where heat transfer results from direct contact between two bodies [2].

In this process of heat transfer, the appropriate rate equation is expressed as

$$q_{conv} = hA(T_s - T_\infty) \quad (2.2)$$

where, q_{conv} is the convective heat transfer rate, h is the convection heat transfer coefficient, T_s is the surface temperature, T_∞ is the fluid temperature and A is the cross-section area across which there is convection [2, 3].

2.3 Lithium-ion Batteries

Lithium-ion batteries have attained a lot of popularity in recent years primarily, due to their high energy density compared to other batteries. Advantages such as energy density and performance at different temperatures are making them more suitable for applications such as Electric vehicles and aviation. Chemistry and performance at different temperatures are discussed below [1].

2.3.1 Lithium-ion Battery Chemistry

Lithium-ion batteries use an intercalated lithium compound as the electrode material. The structure and general operation are described below.

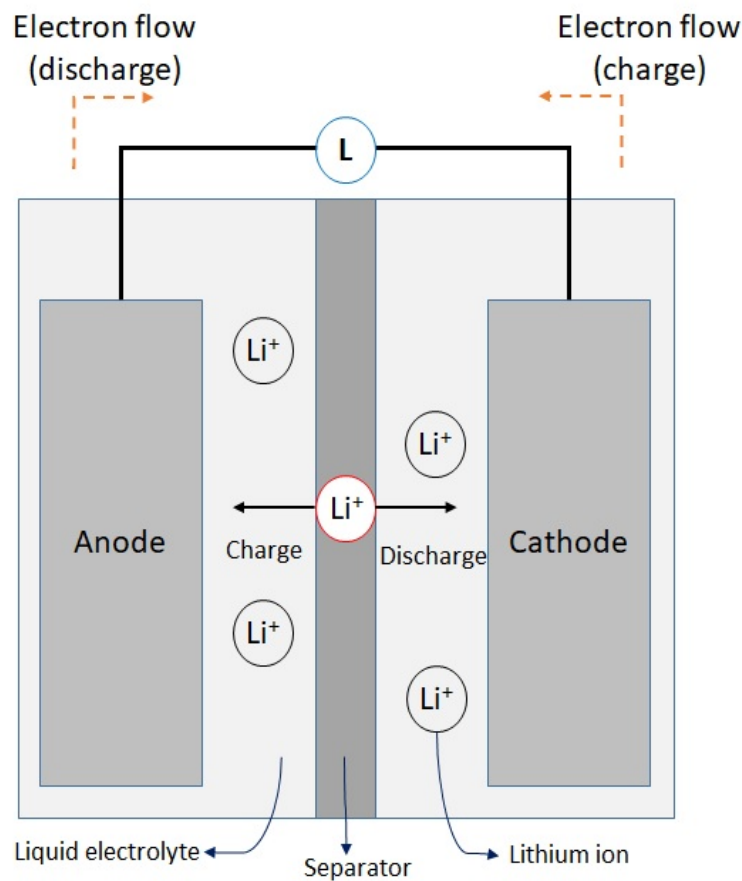


Figure 2.1: Lithium-ion Battery Cell Block Diagram [4]

Figure 2.1 illustrates the four main components of a lithium-ion battery cell, which are a cathode, anode, electrolyte and separator.

Each of these components is effective for the operation of a lithium-ion cell, starting with a cathode, which is made of lithium metal oxide powder and receives lithium-ions from an anode during discharge. A Cathode emits lithium-ions to the anode

during charging. An anode is made out of graphite powder and receives lithium-ions during charging and emits lithium-ions during discharging. The liquid electrolyte helps in transporting lithium ions from the anode to the cathode during the process of charging and discharging. The separator, which is made up of a micro-porous membrane and is necessary to prevent a short circuit between the cathode and the anode [4, 6].

The operation in terms of charging and discharging can be described as shown in Figure 2.1. During the discharging phase, the lithium atoms in the anode interact with the liquid electrolyte losing electrons as well as lithium ions. The electrons from the anode enter the cathode through an external circuit, and the lithium ions enter through the separator. During the charging phase, the lithium ions and electrons move from the cathode to anode in the same way as described in the charging phase. The electron transfer takes place from the positive to the negative electrodes via the load [4, 6].

2.3.2 Types of Battery Structures

Cylindrical: Cylindrical cells are the most popular and widely used batteries over the years in applications such as power tools, medical instruments and laptops. In cylindrical cells, the electrodes are wound tightly and encased in a metal casing, and this process of wounding reduces mechanical vibrations and breaking up of electrode material. The advantages of these cells include cycling ability, long calendar life and ease of manufacturing [8, 9].

Prismatic: Prismatic cells have a box-like structure, which enables them to meet the demands of thinner sizes and lower cost of manufacturing. However, in comparison with cylindrical cell design, prismatic cells are slightly more expensive to manufacture and has lower energy density. The electrodes in a prismatic cell are usually stacked, resulting in a thin profile. For making their mechanical stability comparative to cylindrical cells, prismatic cells require thicker wall size, resulting in a capacity drop [8, 9].

Pouch: The design is similar to a prismatic cell, but in this case, the conductive foil tabs are welded to electrodes and sealed to the pouch carrying the negative and positive terminals. This process enables highly efficient space usage of 90 to 95 % packaging efficiency. This cell structure is simple and lightweight primarily because of the eliminated metal enclosure. This cell structure is gaining importance in applications such as military and automotive industries [8, 9].

2.3.3 Effect of Temperature on Lithium-ion Batteries

Features such as being lighter than other rechargeable batteries, higher energy density and less charge loss over time make lithium-ion batteries better performers than other battery types in EV applications. Yet, there is a need to increase the energy and power density further [5, 7].

Also, in EV applications the battery degradation is a major problem. As battery accounts for a major portion of the cost of an automobile, a battery's lifespan shall be optimized to preserve its power as well as capacity. The three major parameters that affect a battery life span are temperature, State of charge and charging habits [5, 7].

As the temperature is the most relevant to the current study, the effects of temperature on a lithium-ion battery are further elaborated using a case with an LCO electrode [5, 7].

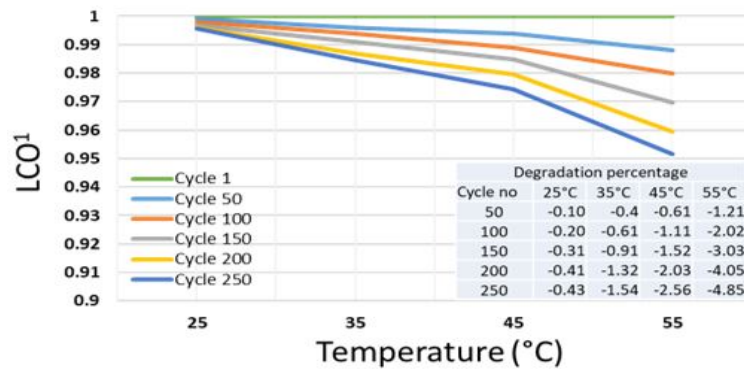


Figure 2.2: LCO electrode degradation as a function of temperature [7]

Figure 2.2 illustrates the degradation of an LCO electrode at different temperatures. From the illustration, it is clear that temperature has a significant effect on the battery cycles. Also, further studies on the degradation concerning ageing have been presented by *Feng Leng, Cher Ming Tan and Michael Pecht*. In their studies, the factors leading to degradation are explained as the formation of surface film and structural changes of the electrode. The reason for the formation of a surface film can be observed as a result of the oxidation at the electrode and electrolyte interface. The structural and phase changes are due to the presence of a surface film, which further lowers the reaction rate in the cell mechanism and thereby results in the change of electrode from hexagonal to cubic phase [5, 7].

2.4 FEA Model

In Finite Element Analysis, physical models are computerized to understand displacement of stress, temperature, fluid flow and other physical behaviour. In this method, the test setup is divided into small parts such as elements called 'finite elements'. These elements are linked to each other through connection points called nodes, and the number of elements describing the degree of freedom associated with the computerized test setup.

2.5 Lumped Parameter Model

In a lumped parameter model, a spatially distributed physical system is simplified into a network topology of discrete entities that resemble the behaviour of the distributed physical system under certain assumptions.

Using an LPN model is the most simple as well as convenient method to solve the transient heating and cooling problems in a system. This can be better explained through the following equation,

$$Bi = \frac{hL}{k} \quad (2.3)$$

where Bi is the *Biotnumber*, L is the length of the solid substance, k is the thermal conductivity of the solid substance, and h is the convection coefficient between the solid substance and fluid [3].

The ratio of heat transfer resistance inside a body to that of the surface as given by the *Biot* number indicates the rate of temperature variance inside a body on application of a thermal gradient to its surface.

For values of $Bi \ll 1$, the heat conduction inside the body is much faster than the heat convection at its surface, and the temperature gradients inside are negligible. Also, the value of $Bi < 0.1$ indicates the applicability of Lumped system analysis to a system with an error rate of less than 5% [3].

2.6 Lumped Parameter Model vs FEA Model

A comparison of Finite Element Analysis and Lumped parameter model is performed considering a cable. This model further enhances our understanding of the LPN and FEA models.

A cable as shown in Figure 2.3 with the dimensions shown in Table 4.1 is considered for the comparison between COMSOL and LPN models in this case.



Figure 2.3: Test cable

2.6.1 COMSOL Model

A COMSOL model for the cable with the dimensions and material properties presented in Table 4.1 is modelled with the following considerations,

All the models are created in 3D and the heat transfer in solids is selected with the study as 'Stationary'.

For geometry, a cylinder block with appropriate dimensions is used to create both the conductor as well as the insulator of the test setup. A copper conductor is created initially, and the EPDM insulation layer is placed over the copper conductor.

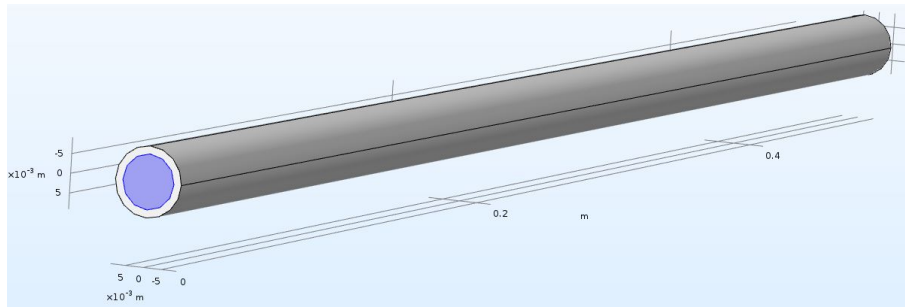


Figure 2.4: COMSOL model of the test cable

The geometry created is assigned the following materials,

- **Copper:** The cylinder block of the conductor is created using this material, and the material is selected from the COMSOL material library [10].
- **EPDM:** The insulation layer, which is placed over the copper conductor is created using this material, EPDM material is selected from the material library [10].

Physics: In this section, the considerations taken in the experiment are applied to the model and is demonstrated by creating a temperature difference of 4°C in the cable.

Under heat transfer in solids (ht), one end of the copper conductor is placed at a temperature of 23 °C and the other at a temperature of 19 °C. The thermal convection coefficient h is set to $10W/(m^2.K)$ at the point where the surface of the cable, especially the insulation layer comes in contact with air. The ambient temperature of the air surrounding the cable is considered to be 19 °C in this case.

A time-dependent study is used to understand the temperature dissipation through different components of the cable setup.

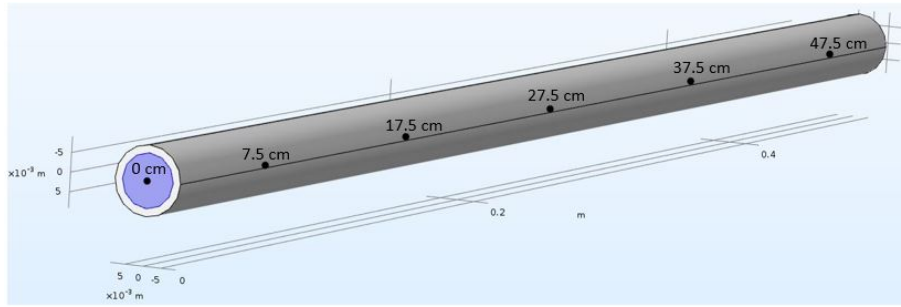


Figure 2.5: COMSOL model with thermal measurement points

Post Processing: To understand the temperature difference, different plots can be created by selecting the locations at which temperature is to be compared with the actual model.

- Five 'Cut point 3D' plots based on sensor location are created. Points at which the temperatures are measured are shown in Figure 2.5.
- Five '1D point graphs' are created to analyze the temperature variations based on sensor location, and the values are noted.

2.6.2 LPN Model

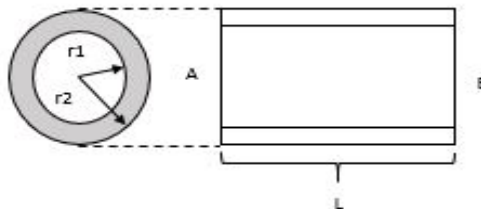


Figure 2.6: Cable block diagram

Figure 2.6 shows a cable with a length $L = 50\text{cm}$. The cable has a conductor of radius r_1 , which is further enclosed by an insulation layer of radius r_2 . Therefore, the inner radius is r_1 and outer radius is r_2 .

A temperature of 23°C , is applied on the side 'A' of the conductor and on the side 'B' the temperature is set to 19°C . The thermal convection coefficient h is set to $10\text{W}/(\text{m}^2.\text{K})$ for the point at which the surface of the insulation layer comes in contact to the air surrounding the cable.

To calculate the heat transfer from side 'A' to side 'B', the 50cm long cable is separated into ten segments of equal length. This segmentation can provide a better estimation of the heat transfer rate across the cable.

From (2.1), the rate of heat transfer during conduction process is expressed as,

$$q_{cond} = \frac{kA}{L}(T_1 - T_2)$$

where k is the thermal conductivity coefficient, A is the cross-section area of the surface that is normal to the direction of heat flow. L is the length of the cable segment, and T_1, T_2 are the temperatures at the hot and cold sides.

To calculate the rate of heat transfer through the cable segment, the thermal resistances of copper conductor, insulator and convection rate at the point of contact between the insulator and air are to be calculated. These calculations are further explained in the following three cases.

Case 1: The thermal resistance of the copper conductor is calculated using the following expression

$$R_{therm1} = \frac{L}{kA} \quad (2.4)$$

where the length $L = 5cm$, the thermal conductivity coefficient $k = 400W/(m.K)$ and the area $A = \pi r_1^2$. Here $r_1 = 0.00708m$. Therefore, the thermal resistance in this case is $0.793K/W$

Case 2:

The thermal resistance of the insulator is calculated in this case. In this case, the heat is flowing through the insulation layer and considering heat transfer in a radial surface [3] the heat transfer rate is expressed as,

$$q_{radial} = -k2\pi rl \frac{dt}{dr} \quad (2.5)$$

and the thermal resistance [10], for conduction in radial surface in this case is expressed as

$$R_{therm2} = \frac{(\ln \frac{r_2}{r_1})}{2\pi lk} \quad (2.6)$$

where r_2 is the radius of the insulation layer, which is $0.00911m$. The thermal conductivity of the EPDM layer is $k = 0.2W/(m.K)$ The thermal resistance in this case is $4.01K/W$.

Case 3:

The thermal resistance [3], between the insulator and air, is calculated in this case. In this case, the heat is transferred from the insulator to the surrounding air, and the thermal resistance for this case is expressed as,

$$R_{therm3} = \frac{1}{hA} = \frac{1}{h2\pi r_2 l A} \quad (2.7)$$

where r_2 is 0.00911cm and thermal convection coefficient $h = 10\text{W}/(\text{m}^2.\text{K})$. The thermal resistance for this case is $34.94\text{K}/\text{W}$.

An LPN model of the cable after calculating the thermal resistance on each of the cases described above is presented in Figure 2.7. In this figure, the total length of the cable is shown with the resistance accounting for each section of the cable. The 5 cm segments shown in Figure 2.7 represent the whole resistance in each section and the resistance division for that particular conductor section, insulator section and convection at the point of contact of air.

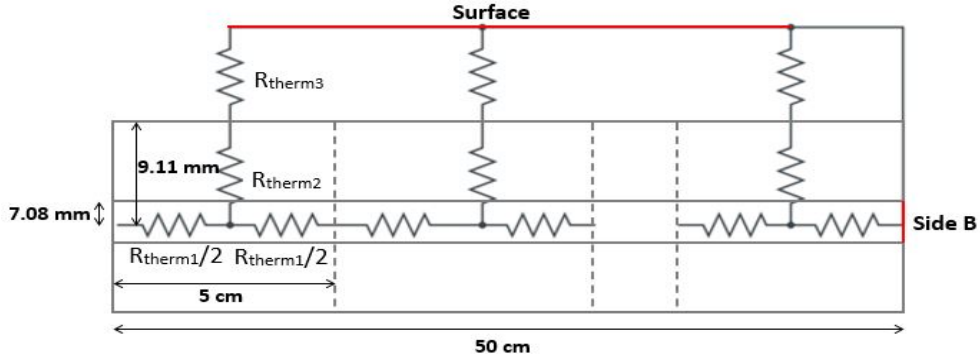


Figure 2.7: Cable LPN structure

2.7 Heat Spreading Angle

The spread of heat depends on the difference between the area of the heat source to that of heat spreading surface. The angle at which the heat is spreading to a large extent relies on the thickness as well as the area of the spreading surface.

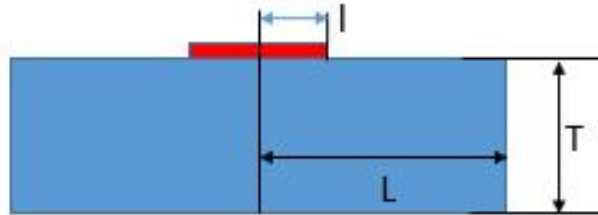


Figure 2.8: Heat spreading angle sample case

From Figure 2.8, let us take $a = \frac{l}{L}$ and $b = \frac{T}{L}$.

The spreading angle for $a < 1$ is usually considered as 45° . However, for very small values of T , this may be different [15].

Also the best fit for $\frac{b}{a} < 1$ is achieved at an angle of 26.6° [16]. The effective

resistance is calculated by placing the heat spread angle in the following formula [16],

$$R_{thermal} = \frac{T}{K * (L + 2 * T * \tan\alpha) * (B + 2 * T * \tan\alpha)} \quad (2.8)$$

where T is the thickness of the surface on which heat is spread, L is the length of that surface, K is the thermal conductivity, α is the heat spreading angle, and B is the breadth of the same surface.

The heat spreading angle of 26.6°C for different thickness values is calculated and verified with the same thickness values in the COMSOL model and the results are compared as follows.

Let us assume that $l = 0.1$ cm, $L = 0.2$ cm and $a = 0.5$ cm. As $\frac{b}{a} < 1$ in most of the cases for selected thickness values, an angle of 26.6°C is considered to calculate $R_{thermal}$.

Table 2.1: Comparison of thermal resistance in COMSOL and LPN models at a heat spreading angle of 26.6°C

All the dimensions are in <i>cms</i> with $l = 0.1$, $L = 0.2$ and $a = 0.5$				
Thickness	$b = \frac{T}{L}$	$R_{thermal}$	From Comsol	Error %
0.01	0.05	0.1597	0.163	2.03
0.015	0.075	0.1163	0.1179	1.34
0.03	0.15	0.0743	0.0713	4.15
0.035	0.175	0.0687	0.0652	5.33

The results indicate an error percentage of 5%, which is good for a general approximation of thermal resistance using heat spreading angle.

3

Base Comparisons

This chapter further elaborates on the comparison of a COMSOL and LPN model through the simplified models shown below.

3.1 Styrofoam Blocks

The entire test setup in this experiment is covered by a styrofoam enclosure and the study of this styrofoam enclosure plays a major role in understanding the temperature distribution in the complete box model.

Thus, different cases of heat transfer in a styrofoam material are observed in a COMSOL model and compared with the corresponding LPN model in this section.

For all the cases in COMSOL, models are created in 3D with a styrofoam material having a thermal conductivity of $0.33 \text{ W}/(m.K)$ [10] and a reference material with an infinite thermal conductivity of $10^6 \text{ W}/(m.K)$. Also, in all cases, the mesh for 3D models is selected as 'Finer' and the study as 'Stationary'.

In the physics section, a temperature difference of 4°C is considered for all cases, and the thermal conductivity is observed in each case by considering different insulation conditions. Finally, the reference dimensions for each case are mentioned in a tabular form.

3.1.1 Case-1

Materials: Styrofoam is the only material used for creating 3D models in this case.

Physics:

- Boundary conditions: To create a temperature difference of 4°C , side A is placed at 22°C and side B at 18°C .
- Thermal Insulation: All sides are thermally insulated except side A and Side B .

Figure 3.1 shows the LPN model and Figure 3.2 shows the COMSOL model

Study Result Explanation: From Figure 3.1 and 3.2 it can be observed that one side of the styrofoam edge is at 22°C and the other side is at 18°C . The thermal

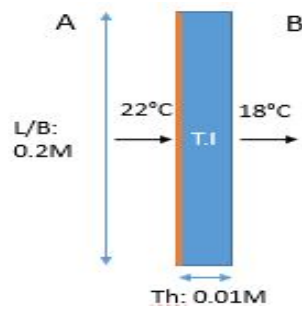


Figure 3.1: Case-1: LPN model setup

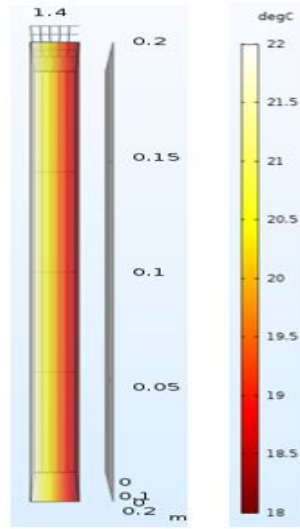


Figure 3.2: Case-1: Temperature distribution in COMSOL model

Table 3.1: Case-1: Heat transfer rate comparison in COMSOL and LPN models

Dimensions (meters)							
Side	Length	Breadth	Thickness	Area	Resistance (K/W)	ΔT ($^{\circ}C$)	Q (W)
B	0.2	0.2	0.01	0.04	7.575	4	0.528
B	Values from the COMSOL design						0.528

conductivity of Styrofoam is $0.033 W/(m.K)$. From Table 3.1, the heat transfer rate from COMSOL design is $0.528 W$, and the calculations resulted in the same value.

3.1.2 Case-2

Materials: 3D models are created using iron and styrofoam materials, in Figure 3.3 the block in *orange*, represents iron and blocks in *blue*, represents styrofoam material.

Physics:

- Boundary conditions: Side *A*, side *B* are at $18^{\circ}C$, and one side of iron is at

22°C.

- Thermal Insulation: All sides are thermally insulated except *A* side of the iron block, side *A* and side *B*.

Figure 3.3 shows the LPN model and Figure 3.4 shows the COMSOL model

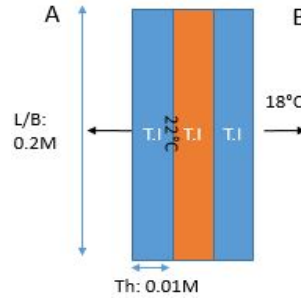


Figure 3.3: Case-2: LPN model setup

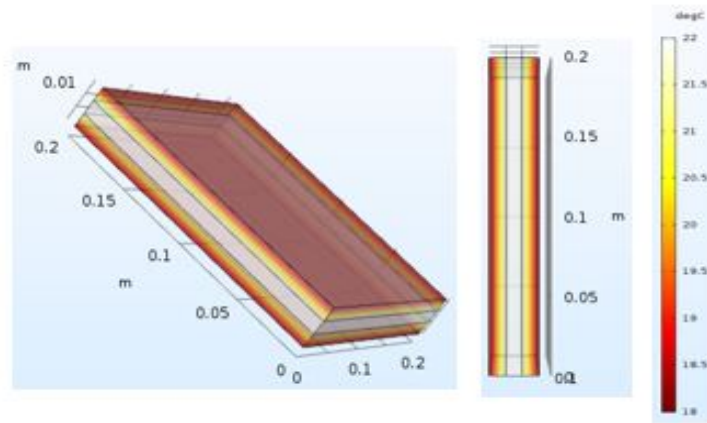


Figure 3.4: Case-2: Temperature distribution in COMSOL model

Table 3.2: Case-2: Heat transfer rate comparison in COMSOL and LPN models

Dimensions (meters)							
Side	Length	Breadth	Thickness	Area	Resistance (K/W)	ΔT (°C)	Q (W)
A	0.2	0.2	0.01	0.04	7.575	4	0.528
B	0.2	0.2	0.01	0.04	7.575	4	0.528
A	Values from the COMSOL design						0.528
B	Values from the COMSOL design						0.528

Study Result Explanation: From Figure 3.3, it can be observed that an iron block is sandwiched between two styrofoam blocks. The side *A* of the iron block is placed at 22°C, and the side *B* of the styrofoam block is kept at 18°C. Except for

side *A* and side *B* all other sides are thermally insulated. From Table 3.2 the heat transfer rate from COMSOL design is 0.528 W and the calculations resulted in the same value.

3.1.3 Case-3

Materials: 3D models are created using iron and styrofoam materials, in Fig. 3.5 the block in *orange* represents iron and blocks in *blue* represents styrofoam materials.

Physics:

- Boundary conditions: side *A*, side *B* are at 18°C, and one side of iron is at 22°C.
- Thermal Insulation: All sides are thermally insulated except *A* side of the iron block, side *A* and side *B*.

Figure 3.5 shows the LPN model and Figure 3.6 the COMSOL model.

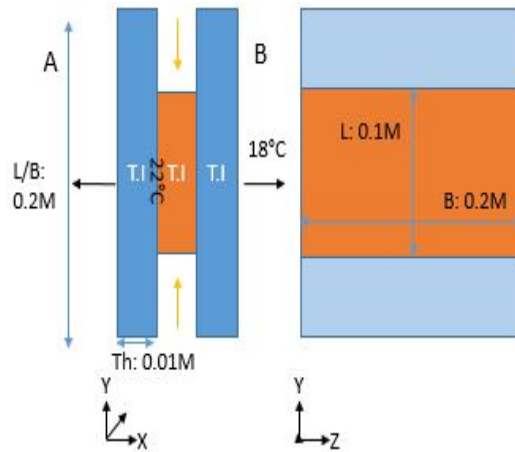


Figure 3.5: Case-3: LPN model setup

Table 3.3: Case-3: Heat transfer rate comparison in COMSOL and LPN models

Dimensions (meters)						
Side	Length	Breadth	Thickness	Area	ΔT (°C)	Q (W)
A (LPN)	0.1	0.2	0.01	0.02	4	0.29
B (LPN)	0.1	0.2	0.01	0.02	4	0.29
A	Values from the COMSOL design					0.293
B	Values from the COMSOL design					0.293

Study Result Explanation: From Figure 3.5, it can be observed that the iron block is not of the same length as that of the styrofoam block. As the length is decreased by 10 cm, the heat spreading angle of 45° (only, in this case, both length

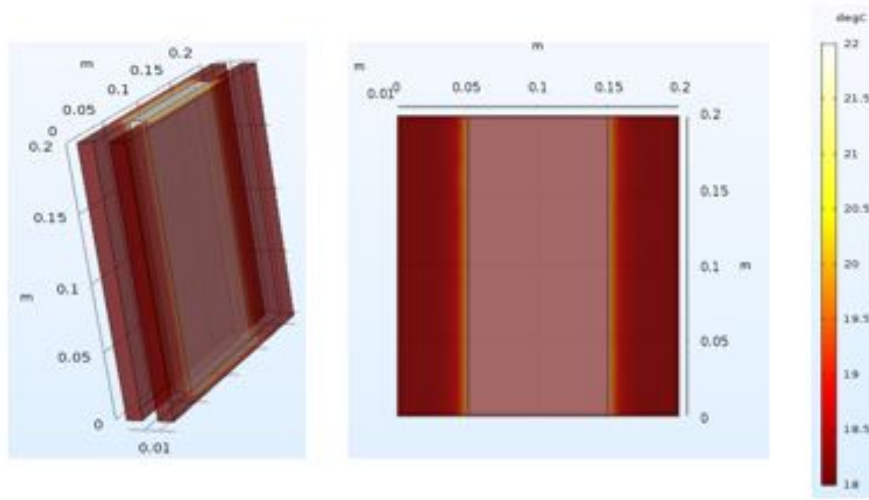


Figure 3.6: Case-3: Temperature distribution in COMSOL model

and breadth are different) is taken into consideration, and the heat transfer rate is calculated for COMSOL as well as LPN model. Both resulted in almost the same value as indicated in Table 3.3.

3.1.4 Case-4

Materials: 3D models are created using iron and styrofoam materials, in Figure 3.7 the block in *orange* represents iron and blocks in *blue* represent styrofoam material.

Physics:

- Boundary conditions: side *A*, side *B* are at 18°C , and one side of iron is at 22°C .
- Thermal Insulation: No side is thermally isolated.

Fig. 3.7 shows the LPN model and Fig. 3.8 the COMSOL model

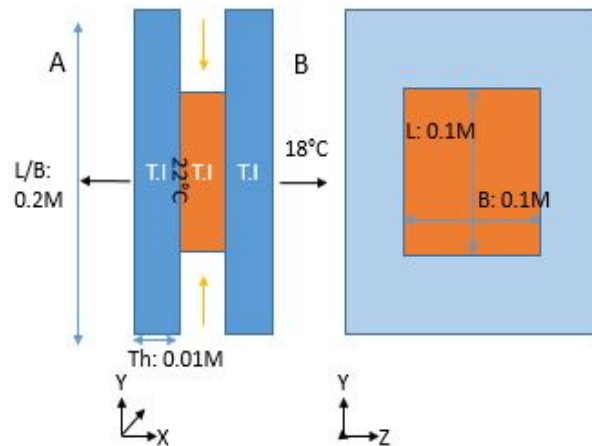


Figure 3.7: Case-4: LPN model setup

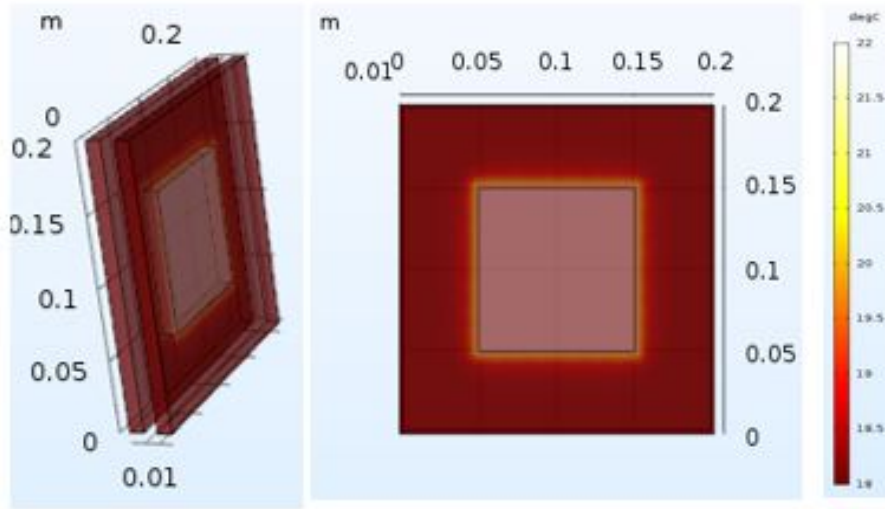


Figure 3.8: Case-4: Temperature distribution in COMSOL model

Table 3.4: Case-4: Heat transfer rate comparison in COMSOL and LPN models

Dimensions (meters)						
Side	Length	Breadth	Thickness	Area	ΔT (°C)	Q (W)
A (LPN)	0.1	0.1	0.01	0.01	4	0.159
B (LPN)	0.1	0.1	0.01	0.01	4	0.159
A	Values from the COMSOL design					0.163
B	Values from the COMSOL design					0.163

Study Result Explanation: From Figure 3.7, it can be observed that both the length and breadth of the iron block are reduced by 10 *cms*. The effective heat transfer rate is calculated from (2.8), by using a heat spreading angle of 26.6°. The effective heat transfer rate resulted in an error of 2%, and the final values are shown in Table 3.4.

3.1.5 Case-5

Materials: 3D models are created using iron and styrofoam materials, in Figure 3.9 the block in *orange*, represents iron and block in *blue* represent styrofoam material.

Physics:

- Boundary conditions: side *A* is at 22°C and side *B* is at 18°C.
- Thermal Insulation: In this case, no side is thermally isolated.

Fig. 3.9 shows the LPN model and Fig. 3.10 shows the COMSOL model

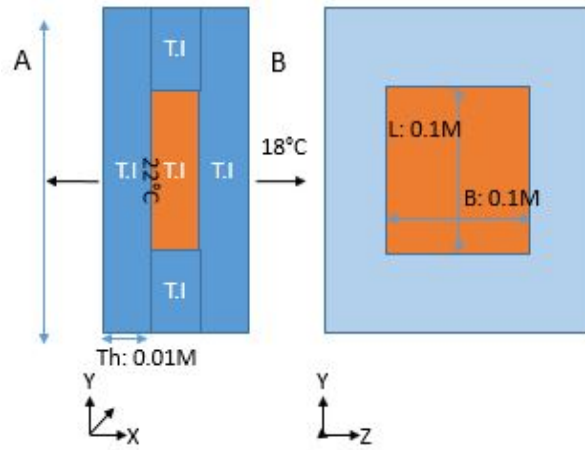


Figure 3.9: Case-5: LPN model setup

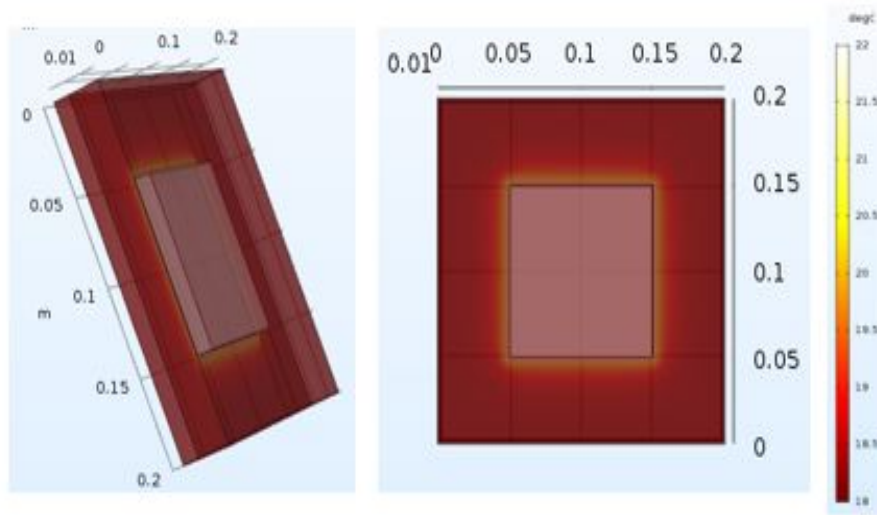


Figure 3.10: Case-5: Temperature distribution in COMSOL model

Table 3.5: Case-5: Heat transfer rate comparison in COMSOL and LPN models

Side	Dimensions (meters)				ΔT (°C)	Q (W)
	Length	Breadth	Thickness	Area		
A	0.1	0.1	0.02	0.04	4	0.188
B	0.1	0.1	0.01	0.04	4	0.159
A+B	Values from the LPN design					0.347
A+B	Values from the COMSOL design					0.361

Study Result Explanation: From Figure 3.9, it can be observed that both the length and breadth of the iron block are reduced by 10 *cms*. The effective heat transfer rate is calculated from (2.8) by using a heat spreading angle of 26.6°. The effective heat transfer rate has resulted in an error of 4%, and the final values are shown in Table 3.5.

3.1.6 Conclusion:

From all the cases presented above comparison of heat transfer in a styrofoam block is performed by considering an LPN model and a COMSOL model. Also, in few cases i.e., in 3, 4 and 5, heat spreading angle is taken into consideration for more accurate estimation.

Thus further cases of the entire test setup and different blocks of the test setup are modelled and compared in a similar manner. All these are presented in the next section. Final results are presented in the results section.

4

Case Setup

This chapter explains a single cell test setup model and details of different components, geometries used in such a model.

4.1 Experiment setup of a cable attached to single cell box model

To evaluate temperature differences between a physical model assembled in a lab and a simulation model prediction, a physical experiment setup is created. In sections 4.2, 4.3 and 4.4, such a physical experiment setup with pictures has been presented with a surrounding temperature of 291.25 K or 18.1°C . Measurements taken from the experiment setups presented in sections 4.3 and 4.4 are compared with COMSOL and LPN models results and are discussed in the next chapter.

The entire case setup can be understood better by starting with the consideration of a cable attached to a sealed box model setup. For all the three models, i.e., a physical experiment setup, a COMSOL model and an LPN model, the temperature values at different points are measured and compared. These sections discussing experiment setups start with defining geometries of each component used in the physical experiment setup, developing a COMSOL model similar to the physical experiment setup using those geometries and finally creating an LPN model of the same. Sections 4.2, 4.3 and 4.4 describe the process in detail.

4.2 Cable

A cable as shown in Figure 4.1 with dimensions shown in Table 4.1 is used in the physical experiment setup.

The cable dimensions are taken from the manufacturer's data sheets [11, 12] and filling factor for the conductor is also calculated based on the manufacturer's data log. The resulting dimensions of conductor and insulator are presented in Table 4.1.



Figure 4.1: Cable used in the test setup

Table 4.1: Cable dimensions from the manufacturers data sheets [11, 12]

Cable with a length 50cm			
Cable section	Material type	Radius (mm)	Thermal conductivity $W/(m.K)$
Conductor	Copper	7.0866	400
Insulator	EPDM	9.118	0.2

4.2.1 COMSOL Model

A COMSOL model for the cable with the dimensions and material properties presented in Table 4.1, is modelled with the following considerations.

Application Mode: 3D, Heat transfer in solids (ht), Time dependent.

Geometry: All components of the enclosed test setup are made up of 3D blocks as shown in Figure 4.2. Initially, a copper conductor and an EPDM insulation layer are created, and the EPDM insulation layer is placed on top of the copper conductor.

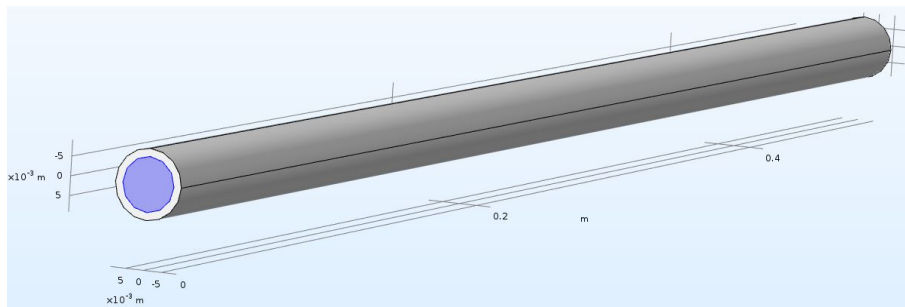


Figure 4.2: Cable: COMSOL model

Materials: The following materials are assigned for creating this geometry,

- **Copper:** A cylinder block is created using this material, and the material is selected from the COMSOL material library.
- **EPDM:** An insulation layer placed on top of the copper conductor is created using this material, and this material is selected from the material library [10].

Physics: Under heat transfer in solids (ht), one end of the copper conductor is at a temperature of 23 °C and the other at a temperature of 19 °C. The thermal convection coefficient h is set to $10W/(m^2.K)$ at the point where the surface of the cable, especially the insulation layer comes in contact with air. In all of the COMSOL models for the cable, the air flow is assumed constant and set to $10W/(m^2.K)$. The ambient temperature of the air surrounding the cable is 19 °C in this case.

Mesh: An extra fine mesh is selected using the Physics-controlled mesh for all domains. Mesh parameters are as follows,

- Number of elements: 90338
- Minimum element quality: 0.2205
- Average element quality: 0.6969
- Mesh volume: 0.02607 cubic meters

Study: A time dependent study is used to understand the temperature dissipation through different sections of the cable setup.

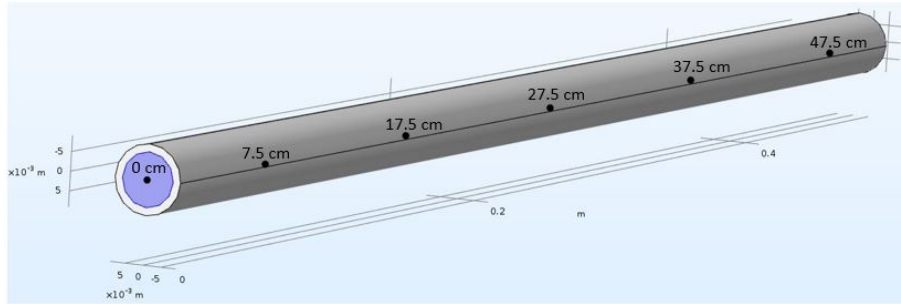


Figure 4.3: Cable: COMSOL model with points of measurement

Post Processing:

- Five 'Cut point 3D' plots based on sensor locations are created. The locations at which the temperature is measured are shown in Figure 4.3.
- Five '1D point graphs' are created to analyze temperature differences based on the sensor location and the temperature values are noted.

4.2.2 LPN Model

Figure 4.4 shows a cable with a length $L = 50cm$. The cable has a conductor of radius r_1 , which is further enclosed by an insulation layer of radius r_2 . Therefore, the inner radius is r_1 and outer radius is r_2 .

A temperature of 23°C is applied on side 'A' of the conductor and, on side 'B' the temperature is 19°C. Thermal convection coefficient h is set to $10W/(m^2.K)$ for the point at which the surface of the insulation layer comes in contact to the air

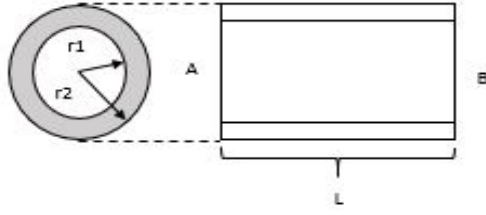


Figure 4.4: Cable: Block diagram

surrounding the cable.

To calculate the rate of heat transfer from side ‘A’ to side ‘B’, the 50cm long cable is further segmented into ten segments of equal length. This segmentation can provide a better estimation of the heat transfer rate across the cable.

From (2.1), the rate of heat transfer during the conduction process is expressed as,

$$q_{cond} = \frac{kA}{L}(T_1 - T_2)$$

where k is the thermal conductivity coefficient, A is the cross-section area of the surface that is normal to the direction of heat flow. L is the length of the cable segment, and T_1, T_2 are the temperatures at hot and cold sides.

To calculate the rate of heat transfer through a cable segment, thermal resistances of the copper conductor, insulator and convection rate at the point of contact between the insulator and air are to be calculated. These calculations are further explained in the following three cases.

Case 1:

The thermal resistance of the copper conductor is calculated using (2.4), where the length $L = 5cm$, the thermal conductivity coefficient $k = 400W/(m.K)$ and the area $A = \pi r_1^2$. Here $r_1 = 0.00708m$. Therefore, the thermal resistance, in this case, is $0.793K/W$

Case 2:

In this case, the thermal resistance of the insulator is calculated. In this case the heat is flowing through the insulation layer and considering heat transfer in a radial surface [3], the rate of heat transfer is expressed as in (2.5) and the thermal resistance [10], for conduction in the radial surface for this case is expressed as (2.6), where r_2 is the radius of the insulation layer, which is $0.00911m$. The thermal conductivity of EPDM layer is $k = 0.2W/(m.K)$. The thermal resistance, in this case, is $4.01K/W$.

The copper conductors thermal resistance is calculated using (2.4), where the length

$L = 5\text{cm}$, the thermal conductivity coefficient $k = 400\text{W}/(\text{m.K})$ and area $A = \pi r_1^2$. Here $r_1 = 0.00708\text{m}$. Therefore, the thermal resistance, in this case, is $0.793\text{K}/\text{W}$

Case 3:

In this case, the thermal resistance [3], between insulator and air, is calculated. The heat from insulator is transferred to the surrounding air, and the thermal resistance is expressed as (2.7), where r_2 is 0.00911cm and the thermal convection coefficient when there is no air flow is assumed to be $h = 10\text{W}/(\text{m}^2.\text{K})$ [?]. The thermal resistance for this case is $34.94\text{K}/\text{W}$.

After calculating the thermal resistance on each of the cases described above, an LPN model of the cable is presented in Figure 4.5. In this figure the total length of the cable is shown with the resistances accounting for each section of the cable. Each 5 cm segments shown in Figure 4.5 represents the whole resistance in each segment and the resistance division for that particular conductor section, insulator section and convection at the point of contact of air.

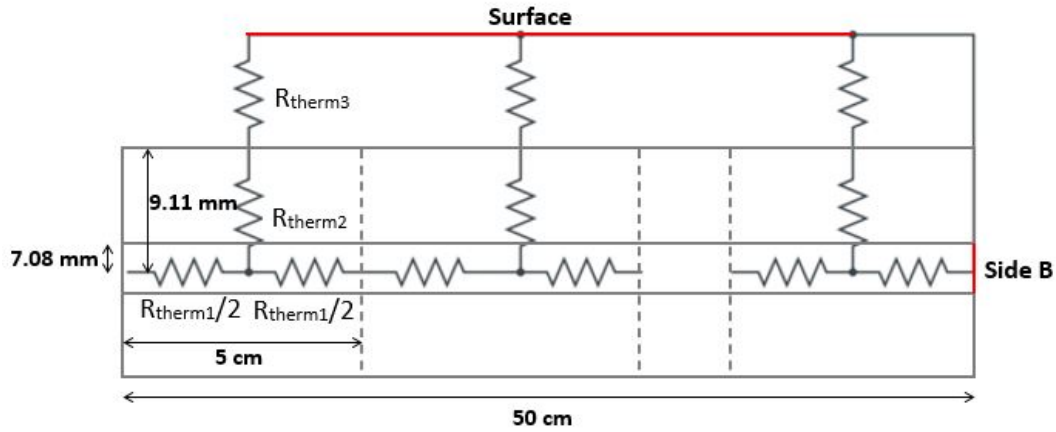


Figure 4.5: Cable: LPN structure

Therefore, the total resistance in each segment of the cable is $R_{tot} = R_{therm1} + R_{therm2} + R_{therm3} = 39.745\text{K}/\text{W}$.

Now the total heat transfer rate is expressed as

$$q_{tot} = (T_1 - T_2)/R_{tot}$$

as the temperature difference is 4°C in this case, the total heat transfer in the cable is as follows,

$$q_{tot} = (T_1 - T_2)/R_{tot} = 0.1\text{W}$$

4.3 Single cell sealed box experiment setup and model

Figure. 4.6 shows the experimental setup of a single cell within a sealed box.

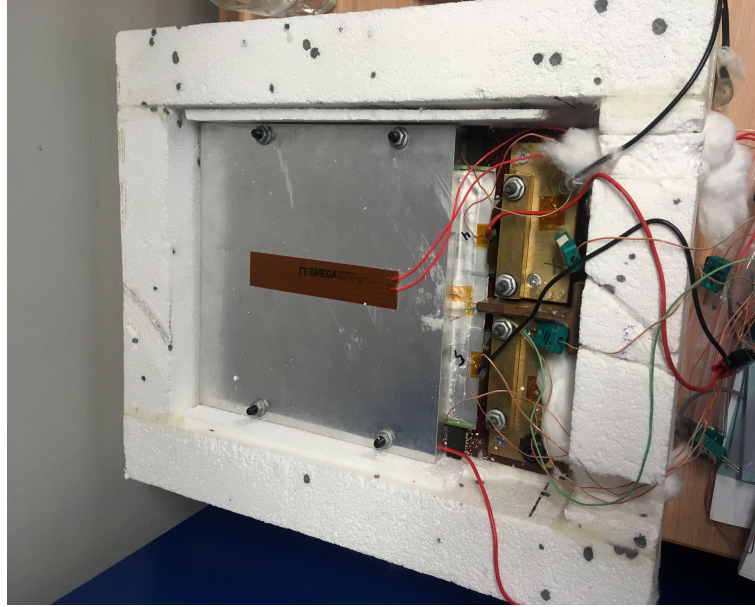


Figure 4.6: Single cell experiment setup

A stacked cell structure can be observed from both the top and front views.

Aluminium plates surround the top and bottom of the single cell. The positive and negative electrodes of the cell are connected to a pair of brass bars on the positive as well as the negative side through tabs. The brass bars are further tightened together through the bolts, as shown in Figure 4.6.

A bakelite plate of relevant size is supporting the bottom aluminium plate. A heating mat is placed on an aluminium plate surrounding the top portion of the cell.

This setup of stacking the aluminium plates, cell, bakelite plate and connecting cell to the brass bars through extended tabs is referred to as the 'Test setup'.

The test setup is enclosed by thick walls of styrofoam as well as filled with cotton to have better insulation and to prevent air leakages.

The heating mat acts as a heat source and sensors are placed on various positions to measure respective temperatures during the charging process.

The model shown in Figure 4.6 is made up of several components. Therefore, modelling of the test setup using COMSOL and LPN are done in multiple steps.

- Box model with cell and aluminum blocks

- Box model with test setup

4.3.1 Box model with cell and aluminum blocks

In this case, a single cell with aluminium blocks on top and bottom is taken. A styrofoam box is covering this setup. This model helps in understanding the temperature differences across the styrofoam box used in the experiment setup. A COMSOL and an LPN model of the box setup are created and the results are compared.

4.3.1.1 COMSOL model

A COMSOL model for the experiment setup stated in section 4.3.1, is modelled with the following considerations.

Application Mode: 3D, Heat transfer in solids (ht), Time dependent.

Geometry: All the components of the enclosed experiment setup are created using 3D, as shown in Figure 4.7. A block function with appropriate dimensions is used to create all the key components of the experiment setup. A bakelite block is created initially and an aluminium plate block, furthermore cell blocks are stacked on it. For the styrofoam setup, two individual blocks, one covering the top portion of the experiment setup and the other covering the entire test setup are created.

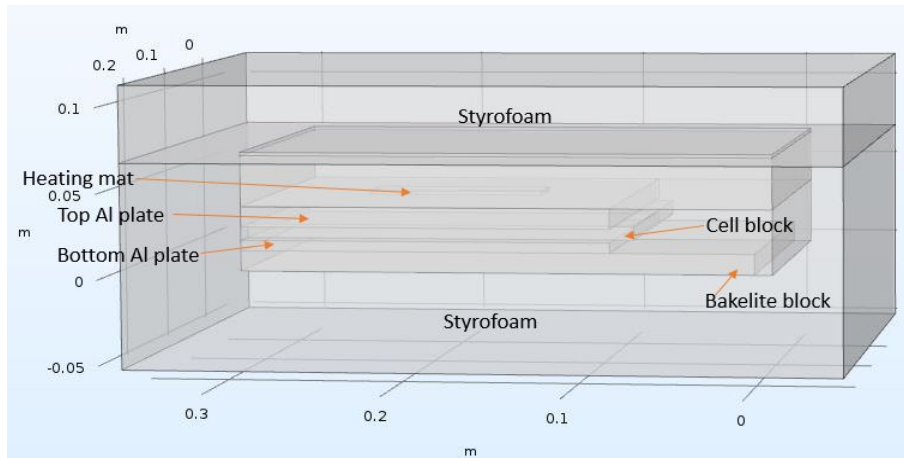


Figure 4.7: Battery box: COMSOL model with partial test setup

Materials: The following material properties are assigned to the geometry created in Figure 4.7.

- Aluminum: Two plate blocks, that cover top and bottom portions of the cell and the heating mat placed over the top aluminium plate are created using this material.
- Bakelite: The plate block, that is located in between the bottom styrofoam enclosure and bottom aluminium plate is created using this material. Also the cell block is created using this material and it is selected from the user material data [10].

4. Case Setup

- **Styrofoam:** The top and bottom blocks covering the experiment setup forming an enclosure are created using this material. The material is selected from the user material data [10].
- **Air:** The rest of the whole box setup is filled with air. The properties are selected from the COMSOL material library.

Physics: Under heat transfer in solids (ht), the temperature for the entire outer portion of the box is considered as 291.25 K or 18.1°C . A heating mat is considered as a heat source and a heat rate of 2.4 Watts , is given as an input to the heating mat. The outer portion of the box is thermally insulated and no form of convection is taken into account.

Mesh: A fine mesh is selected in the physics-controlled mesh for all domains. The mesh parameters are as follows

- Number of elements: 244707
- Minimum element quality: 0.1541
- Average element quality: 0.621
- Mesh volume: 0.02178 cubic meters

Study: A 'Stationary' study is selected for this case to understand the temperature dissipation through the different components of the box setup.

Post Processing:

- Four 'Cut point 3D' plots based on sensor location are created. The locations are shown in Figure 4.8, the points are located on the heating mat, on the center of the cell block, at the top of the bakelite block and on top of the bottom styrofoam block.

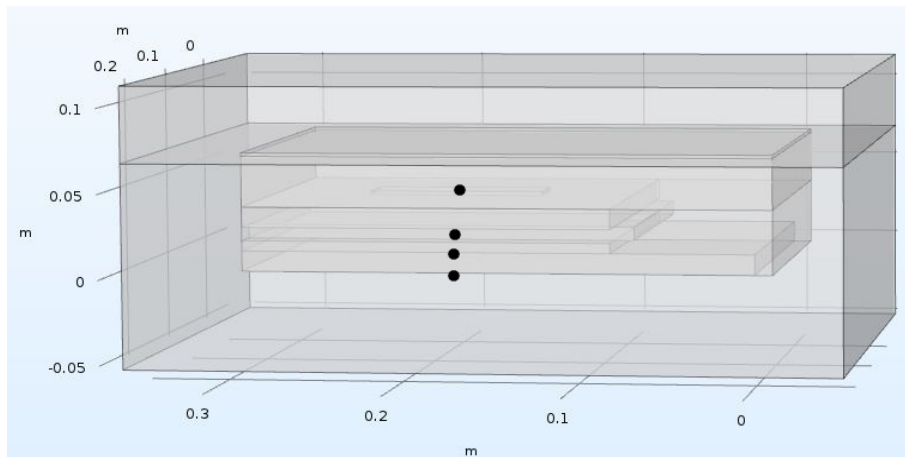


Figure 4.8: Battery box: COMSOL model with points of measurements

- Four '1D point graphs' are created to analyze temperature variations based on the sensor locations and the values are noted.

4.3.1.2 LPN Model

Figure 4.9 shows the arrangement of different components in the box considered for this test case. Also, the setup considered here is related to the physical test setup of the single-cell box model.

In this box model, the heating mat acts as a heat source at which a heat transfer rate of 2.4 W is applied. The heating mat is presented in *red* and is arranged over the aluminium plate. The cell is in *blue* and is enclosed by aluminium plates on the top as well as the bottom. The aluminium plates that are placed on top and bottom portions of the cell are shown in *maroon*. A bakelite plate is placed at the bottom of the whole setup of the aluminium plates and shown in colour *black*. Further, the entire arrangement of Aluminum plates, cell, and bakelite plate is enclosed by a styrofoam layer on all four sides. The ambient temperature surrounding the box model, in this case, is 291.25 K or 18.1°C similar to that of the COMSOL model.

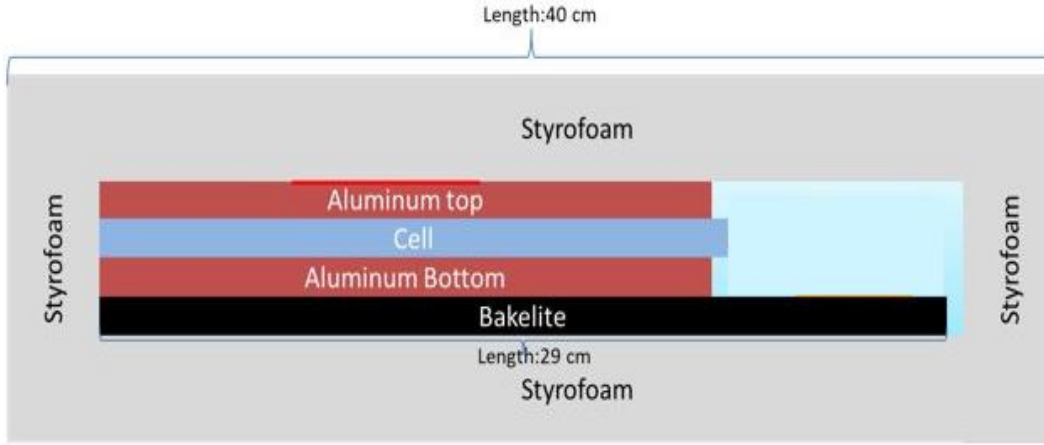


Figure 4.9: Box: LPN model with partial test setup

The dimensions of different components of the box model are presented in Table 4.2. To better understand the temperature distribution, in this case, the thermal conductivity k of the cell is considered to be the same as that of bakelite, which is 0.2 W/mK instead of the actual value. Thus the calculations in this test case are carried out assuming the same thermal conductivity cell and bakelite blocks to better understand the temperature variations in the styrofoam block.

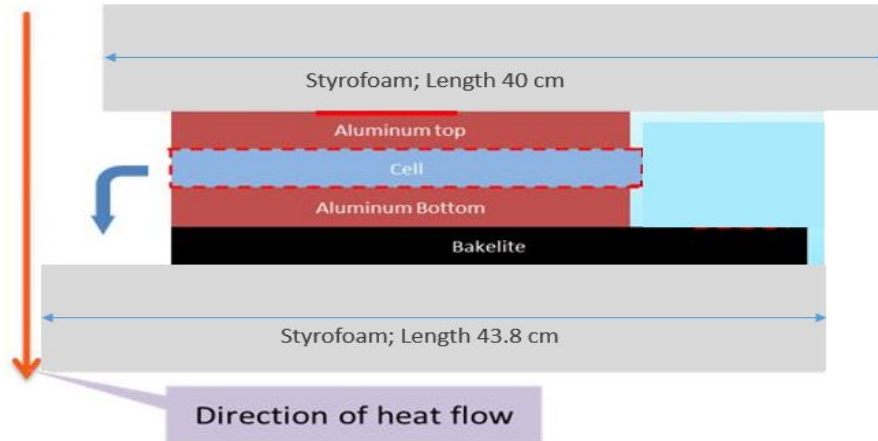
In the box model shown in Figure 4.9 air occupies an area of approximately 25 cm^2 . Though this is a significant portion in this box setup, heat transfer due to convection is not considered assuming the nature of airflow as stagnant within the closed box setup. Also, conduction through the air is considered negligible primarily due to the direction of heat flow, which is from heating mat towards the bakelite plate. Thus, heat flow is considered only in the Y direction in this case.

Figure 4.10 illustrates the modifications made to the box model for building an

Table 4.2: Battery box model: Dimensions of different components

Component type	Length (in X direction) in <i>cm</i>	Breadth (in Z direction) in <i>cm</i>	Width (in Y direction) in <i>cm</i>	Thermal conductivity (<i>k</i>)
Styrofoam top	40	33	7.5	0.033
Aluminum top	20.9	20.9	1.2	238
Cell	22	17	0.8	0.2
Aluminum bottom	20.9	20.9	0.6	238
Bakelite	29	20.9	1.2	0.2
Styrofoam bottom	40	33	5.2	0.033

LPN model. As the heat flow is primarily considered to be only in *Y* direction, the styrofoam enclosing sections other than the top and bottom are assumed to be unfolded as shown in Figure 4.10 and the equivalent resistance of the whole block is calculated. The rate of heat transfer is assumed to be negligible in the portion occupied by air and the styrofoam enclosure located next to it.

**Figure 4.10:** Battery box model (Side view)

The thermal resistance in each component is calculated following the modifications shown in Figure 4.10. Also, a heat spreading angle $[26.6^\circ]$ is considered for the thermal resistance calculations of the styrofoam block located on top of the heating mat as well as for the aluminium plate located just below the heating mat. An LPN model, with the thermal resistances for all the components in the test setup, is shown in Figure 4.11. Red dots indicate the node connections between the thermal resistances of different components.

The thermal resistance can be calculated using (2.1).

The thermal resistance for each component is calculated and presented in the form of a network model and is shown in Figure 4.12.

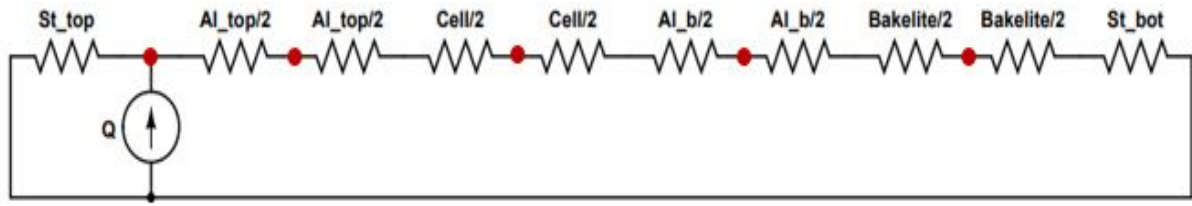


Figure 4.11: LPN circuit of battery box model with partial test setup

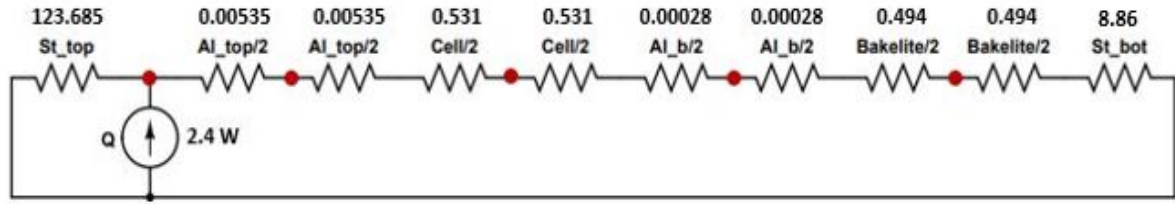


Figure 4.12: Battery box LPN circuit with temperature at different locations

Now the thermal resistance for each component in the box setup is known, the temperature can be determined using nodal analysis at the node located near the heating mat

$$-2.4 + \frac{T_1}{123.685} + \frac{T_1}{10.92} = 0$$

where T_1 is the temperature at the node point at the heating mat, $123.685 K/W$ is the thermal resistance of the styrofoam located at the top of the aluminium plate and heating mat. $10.92 K/W$ is the combined thermal resistance of all other components in the test setup.

The temperature at T_1 and other nodes is compared to a COMSOL model of the same setup and the results are presented in the next chapter.

4.3.2 Box Model with Test Setup

This section presents the physical box model with the entire test setup included and, both the COMSOL and the LPN models of the same are shown below.

4.3.2.1 COMSOL Model

A COMSOL model for the physical experiment setup stated in section 4.3 is modelled with the following considerations.

Application mode: 3D, Heat transfer in solids (ht), Time dependent.

Geometry: All components of the enclosed experiment setup are created using 3D, as shown in Figure 4.13. A block function with appropriate dimensions is used to create all the key components of the experiment setup. The bakelite block is created initially and the aluminium plate block, cell block and brass bar blocks are stacked on it accordingly. For the styrofoam setup two individual blocks, one covering the top portion of the test setup and the other covering the entire test setup are created.

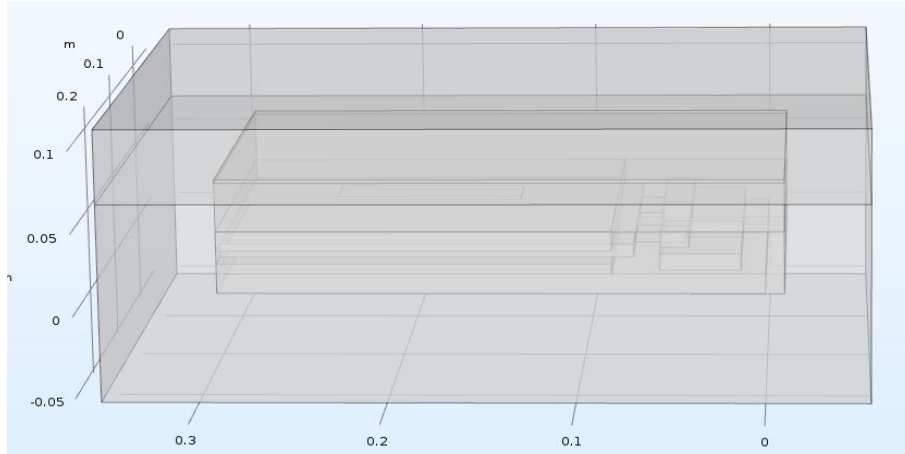


Figure 4.13: Battery box: COMSOL model with complete experiment setup

Materials: The following materials are assigned to the geometry presented in 4.13,

- **Aluminium:** Aluminium is used to create the aluminium plates. This material is selected from the material library.
- **Brass:** Brass is used to create four brass bars, one pair for the positive electrode and the another for the negative electrode. This material is selected from the user material data [10].
- **Bakelite:** Bakelite is used to create a bakelite plate. This material is selected from the user material data [10].
- **Styrofoam:** Styrofoam is used to create the top block covering the test setup and enclosure. This material is selected from the user material data [10].
- **Air:** The rest of the box setup except the cell block is filled with air. The material for cell block is selected from the user material data [10].
- **Cell:** As the cell materials are not usually known, the parameters such as thermal conductivity and heat capacity of the cell are selected from one of the studies [17]. All the necessary cell parameters are selected from this study and used in modeling all the COMSOL models.

Physics: Under heat transfer in solids (*ht*), the temperature for the entire outer portion of the box is considered to be 291.25 K or 18.1°C . The heating mat is considered as the heat source and the respective heat rate of 2.4 Watts is given as an input to the heating mat.

Mesh: A fine mesh is selected in the Physics-controlled mesh for all domains and the mesh parameters are as follows

- Number of elements: 125356
- Minimum element quality: 0.00365
- Average element quality: 0.5906
- Mesh volume: 0.0219 cubic meters

Study: A 'Stationary' study is used to understand the temperature dissipation through different components of the test setup.

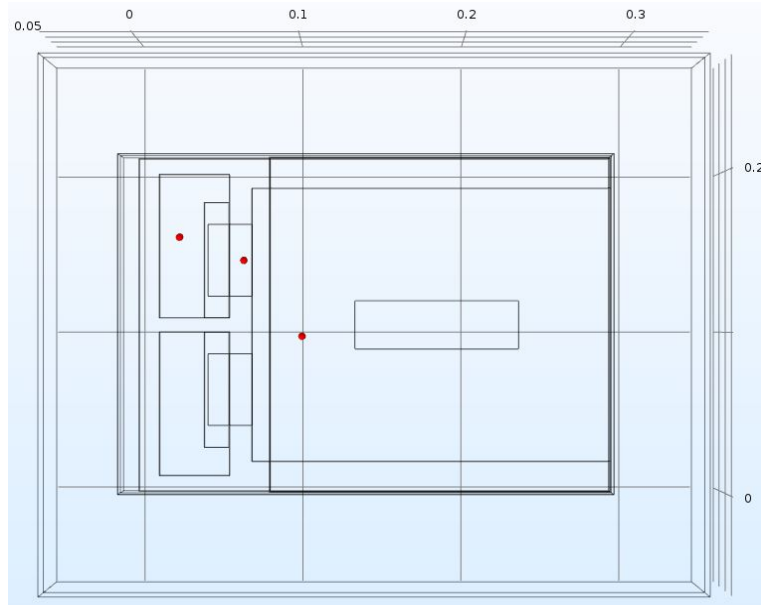


Figure 4.14: Battery box: COMSOL model with points of measurement

Post processing:

- Three 'Cut point 3D' plots based on the sensor location are created. The Sensors are located on the aluminium plate, brass bar and on the positive tab, as shown in Figure 4.14.
- Three '1D point' graphs are created to analyze temperature differences based on the sensor location.

4.3.2.2 LPN model

A Single-cell and an experiment setup of the cell along with different components used in the setup are described in this section.

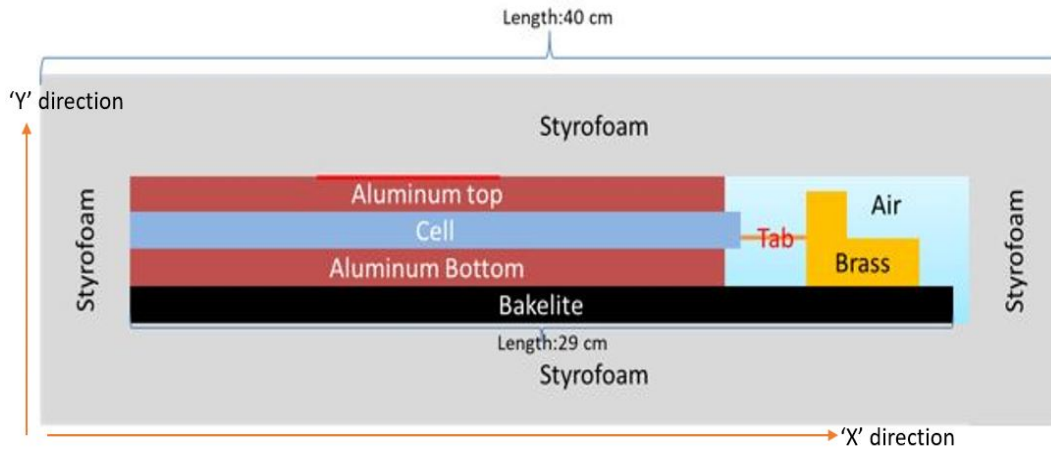


Figure 4.15: Battery box model of a single cell

From Figure 4.15, the arrangement of different components in a single cell battery box can be observed. The heating mat in *red* acts as a heat source in this arrangement and is placed over the aluminium plate. The cell in *blue* is enclosed by aluminium plates on top as well as on the bottom. One end of the cell in *X* direction, is connected to the brass bar through a tab and the other end is enclosed by a styrofoam wall. A bakelite plate is placed at the bottom of the whole setup of the aluminium plates, cell and brass bar as indicated in Figure 4.15 above. Further, the entire setup of the aluminium plates, cell, brass bar and bakelite plate is enclosed by a styrofoam layer on all the four sides.

The dimensions of different components of the box model are given in Table 4.3. To better understand the temperature differences due to the presence of an air gap between multiple components in the test setup, the test setup of the LPN model is subdivided.

Division of the box model: The box model is further divided into two parts

- **Simple model:** In this model, heat flow is considered only in the *Y* direction. Therefore, the area of the cell is considered as a combination of the cell, tab and brass bars. The thermal resistance and capacitance are also selected as per the heat flow in the *Y* direction.

Table 4.3: Dimensions of different components in the box

Component type	Length (in X direction) in <i>cm</i>	Breadth (in Z direction) in <i>cm</i>	Width (in Y direction) in <i>cm</i>
Styrofoam top	40	33	7.5
Aluminum top	20.9	20.9	1.2
Cell	22	17	0.8
Aluminum bottom	20.9	20.9	0.6
Bakelite	29	20.9	1.2
Styrofoam bottom	40	33	5.2

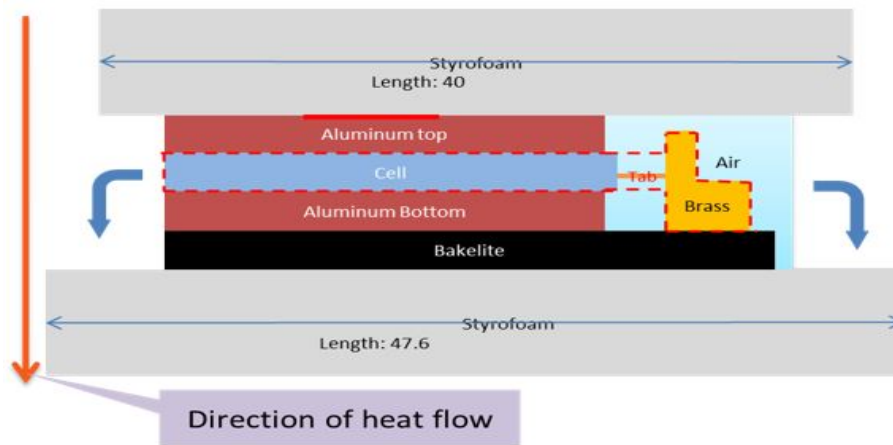
- **Complex model:** In this model the box is cut into two halves, heat is in *Y* direction in one half and both *X*, *Y* directions in the other half. These two parts are explained separately with figures.

These two halves are implemented in an LPN model and the division is described in the following sections.

4.3.2.3 LPN model: Simple model

The need for the development of a simple model is further explained in this section along with materials, geometric properties and the resulting LPN models.

In this model, the heat flow is considered only in one direction, and that is in the *Y* direction. Therefore, the cell area is considered as a combination of cell, tab and brass bars. The thermal resistance and capacitance are also selected as per the heat flow in the *Y* direction.

**Figure 4.16:** Simple model: Battery box model (Side view)

The dimensions of different components of the simple model are shown in Table 4.4. The thermal resistance for each component in Figure 4.16 can be calculated using (2.4). The calculated values are presented in the Table 4.5.

4. Case Setup

Table 4.4: Simple model: Dimensions of different components

Component type	Length (in X direction) in <i>cm</i>	Breadth (in Z direction) in <i>cm</i>	Width (in Y direction) in <i>cm</i>
Styrofoam top	40	33	7.5
Aluminum top	20.9	20.9	1.2
Cell	27.7	17	0.8
Aluminum bottom	20.9	20.9	0.6
Bakelite	29	20.9	1.2
Styrofoam bottom	40	33	5.2

Table 4.5: Simple model: Thermal resistance calculations

Component type	Length <i>cm</i>	Breadth <i>cm</i>	Area in <i>meters</i>	Thermal conductivity $W/(m.K)$	Height <i>cm</i>	$R_{thermal} K/W$
Styrofoam top	40	33	0.132	0.033	7.5	17.218
Aluminum top	20.9	20.9	0.044	238	1.2	0.001
Cell _y	27.7	17	0.047	0.5 [17]	0.8	0.338
Aluminum bottom	20.9	20.9	0.044	238	0.6	0.001
Bakelite	29	20.9	0.061	0.2	1.2	0.99
Styrofoam bottom	47.6	40.6	0.193	0.033	5.2	8.154

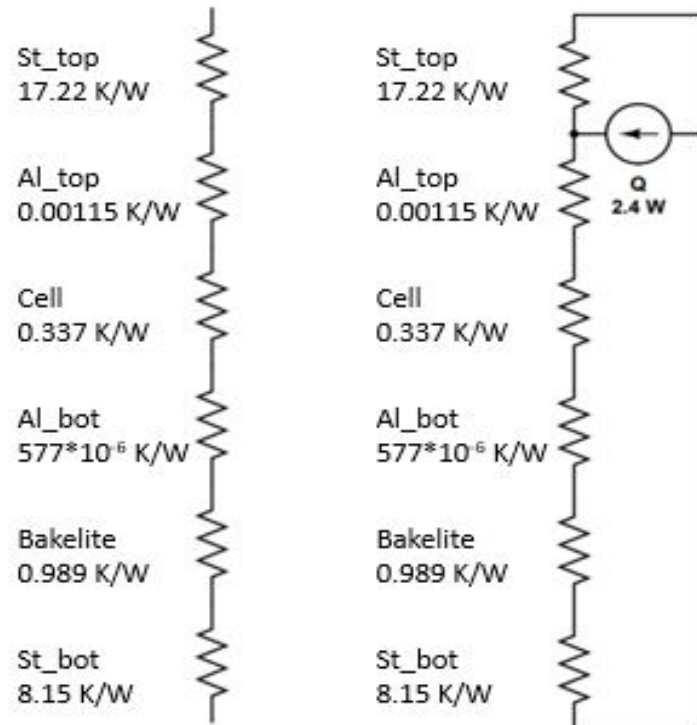


Figure 4.17: Simple model: Thermal resistance network from Table 4.5

The thermal capacitance of the simple model can be calculated from the ‘mass’ and ‘Heat capacity’ of each component. Table 4.6 shows the heat capacity values for each component.

Table 4.6: Simple model: Thermal capacitance calculations for different components

Component type	Density g/cm^3	Length cm	Breadth cm	Height cm	Volume	Mass kg	Heat capacity $J/(kg.K)$	Thermal capacity $C_p * m$
Styrofoam top	0.035	40	33	7.5	9900	0.3465	1131	391.89
Aluminum top	2.7	20.9	20.9	1.2	524.172	1.415	900	1273.73
Cell	2.368	17.1	22	0.8	300.96	0.712	1091 [17]	777.526
Aluminum bottom	2.7	20.9	20.9	0.6	262.086	0.707	900	636.86
Bakelite	1.3	29	20.9	1.2	727.32	0.945	920	869.87
Brass top	8.5	7.2	1.5	1	10.8	0.0918	380	34.884
Brass bottom	8.5	9	4.3	1	38.7	0.328	380	125
Styrofoam bottom	0.035	40	33	5.2	6864	0.24	1131	271.71
Tab	8.96	2.7	4.5	0.02	0.243	0.0021	900	1.959

LPN model considering resistance and capacitance for the simple model is as shown below.

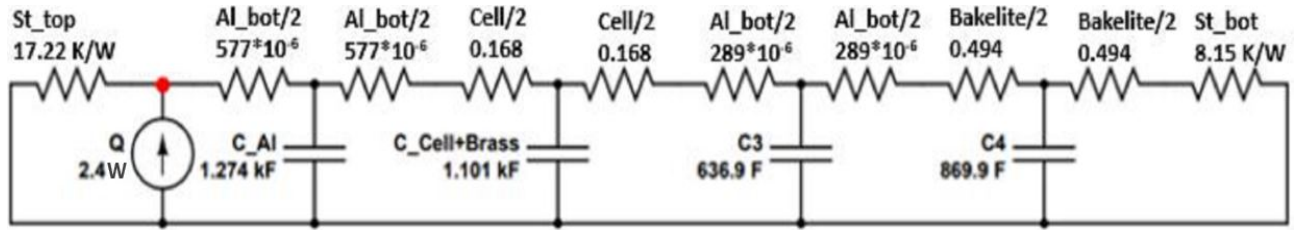


Figure 4.18: Simple model: LPN circuit

At the node indicated in ‘red’, the temperature can be calculated as follows using nodal analysis,

When the capacitor is not at all charged, i.e., at time $t = 0$,

$$-2.4 + \frac{T_1}{17.22} + \frac{T_1}{9.48} = 0$$

Therefore, $T_1 = 14.67$ °C where 17.22 K/W is the resistance of the styrofoam top and 9.48 K/W is the sum of all individual resistances from aluminium top to styrofoam bottom. The resulting effective resistance is 6.114 K/W.

4.3.2.4 LPN model: Complex model

In this model, the box is cut into two halves, the flow of heat is in the Y direction in one half and both X , Y directions in the other. These two parts are separately explained with figures.

Separation of two sections in the complex model is shown in the figure below.

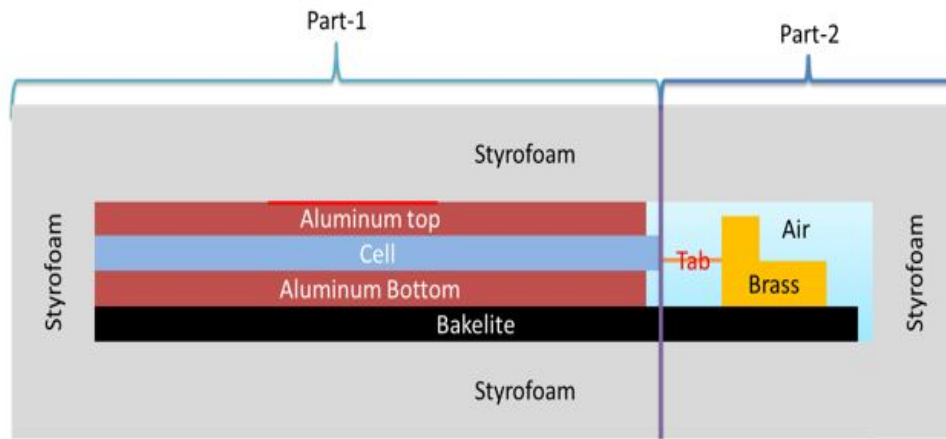


Figure 4.19: Separation of box model into two parts

From Figure 4.19, it can be observed that the box is now separated into two parts. In part 1, the majority of the heat flow is in the Y direction similar to the simple model. In part 2, the heat flow is in both X and Y directions.

Part-1

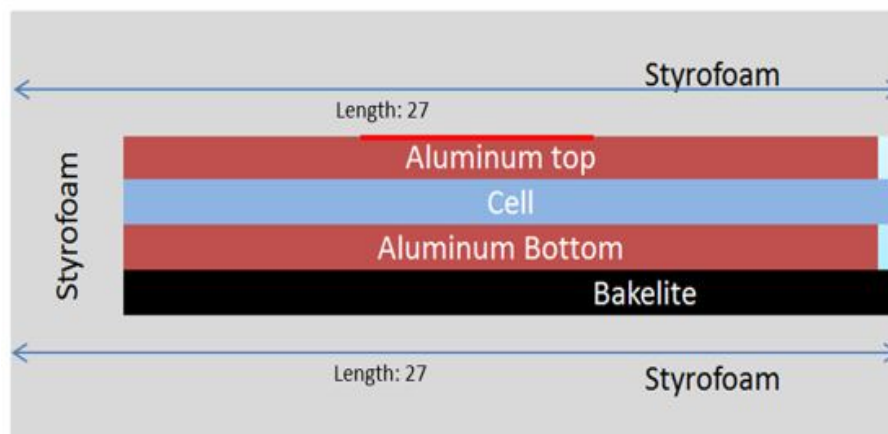


Figure 4.20: Part 1 of the complex box model

Figure 4.20, describes part-1 of the complex model. In this part, the section from tab till brass is separated from the experiment set up and the heat flow is considered only in the Y direction. Also, heat flow from cell to the brass pieces is shown below.

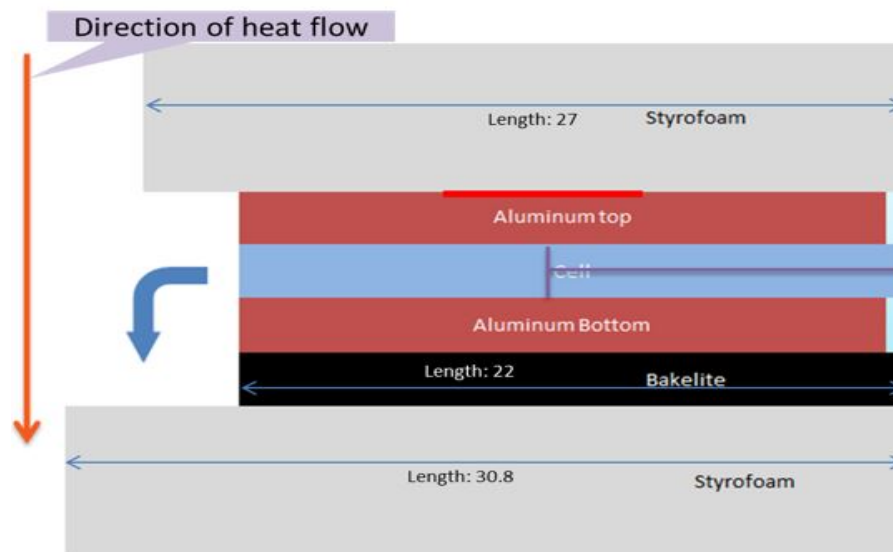


Figure 4.21: Part 1 of the complex model in the X direction (Side view)

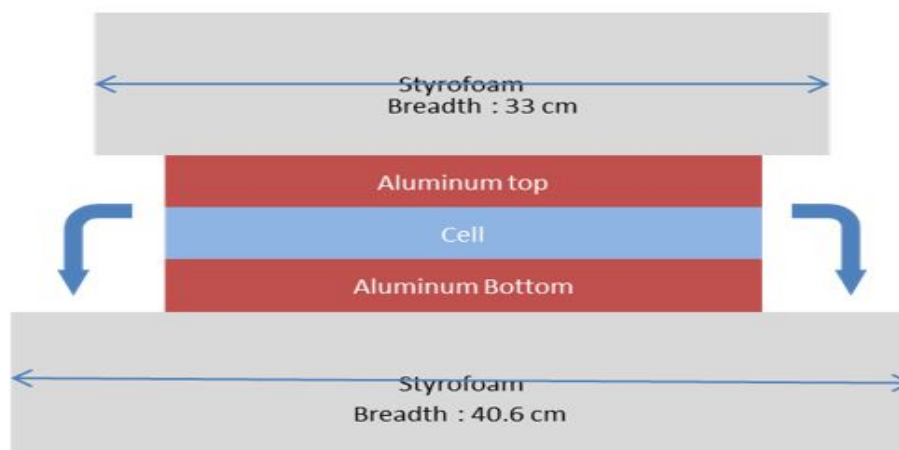


Figure 4.22: Part 1 of complex model in the Z direction (Front view)

From Figures 4.21, 4.22, the thermal resistance of each component can be calculated using the dimensions as shown in Table 4.7.

4. Case Setup

Table 4.7: Part 1: Thermal resistance calculations of different components

Component type	Length <i>cm</i>	Breadth <i>cm</i>	Area in <i>m</i>	Thermal conductivity <i>W/(m.K)</i>	Height <i>cm</i>	$R_{thermal} K/W$
Styrofoam top	27	33	0.089	0.033	7.5	25.507
Aluminum top	20.9	20.9	0.044	238	1.2	0.001
Cell _{Ydirection}	17.1	22	0.037	0.5 [17]	0.8	0.425
Cell _{Xdirection}	17.1	0.8	0.0013	29 [17]	11	2.772
Aluminum bot- tom	20.9	20.9	0.044	238	0.6	0.00057
Bakelite	22	20.9	0.046	0.2	1.2	1.3
Styrofoam bot- tom	30.8	40.6	0.125	0.033	5	12.11

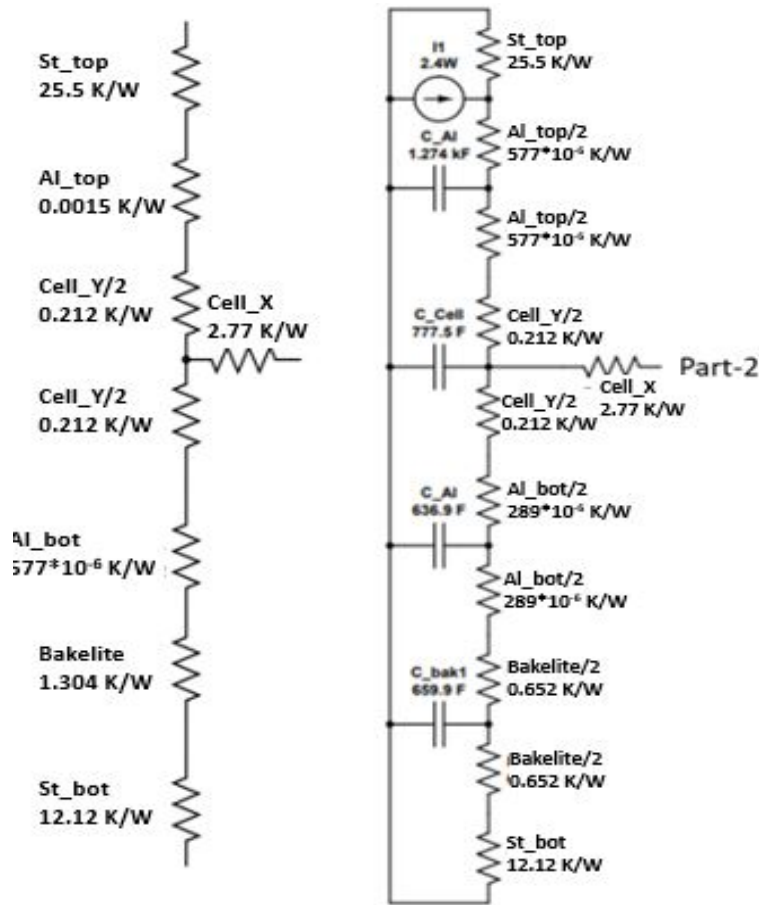


Figure 4.23: Thermal resistance network of the complex model part-1 from Table 4.7

Part-2

From Figure 4.24, it can be observed that in part 2, more elements are to be considered to calculate the thermal resistance. The following adjustments are made to

simplify these calculations,

1. Air medium is combined with styrofoam on both X and Y direction and is shown in Figure 4.25.
2. The air below the tab is not considered in this evaluation of thermal resistance calculation.

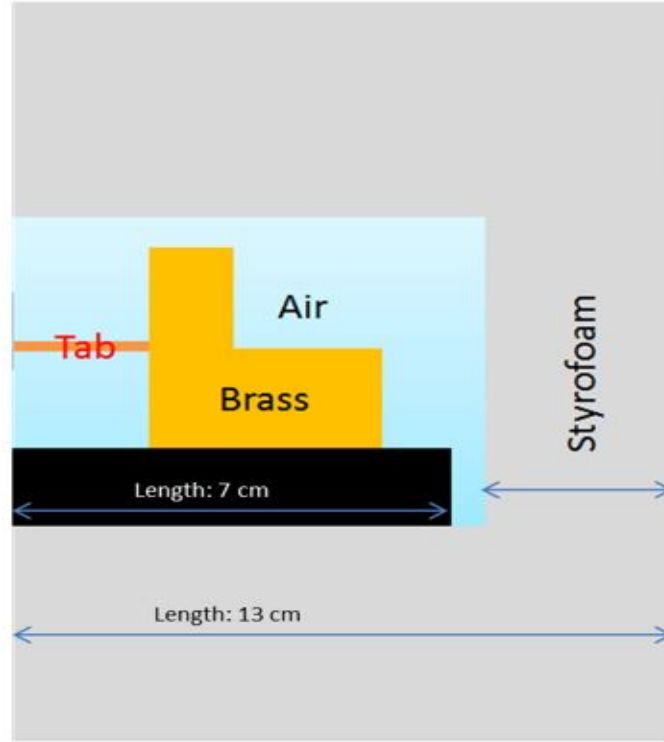


Figure 4.24: Part-2 of the complex model

All adjustments are shown in Figure 4.25, in red and orange dotted lines. In both cases, the effective thermal resistance will be the resistance resulting from a combination of air and styrofoam thermal conductivity.

The effective thermal conductivity of the box in orange dotted lines is calculated as follows,

$$\frac{L_{eff}}{K_{eff} * A_{eff}} = \frac{L_1}{K_1 * A_1} + \frac{L_2}{K_2 * A_2}$$

$$\frac{6.5}{K_{eff} * 3.8 * 20.9} = \frac{5}{0.033 * (3.8 * 20.9)} + \frac{1.5}{0.02 * (3.8 * 20.9)}$$

Therefore $K_{eff} = 0.0286 \text{ W}/(m.K)$

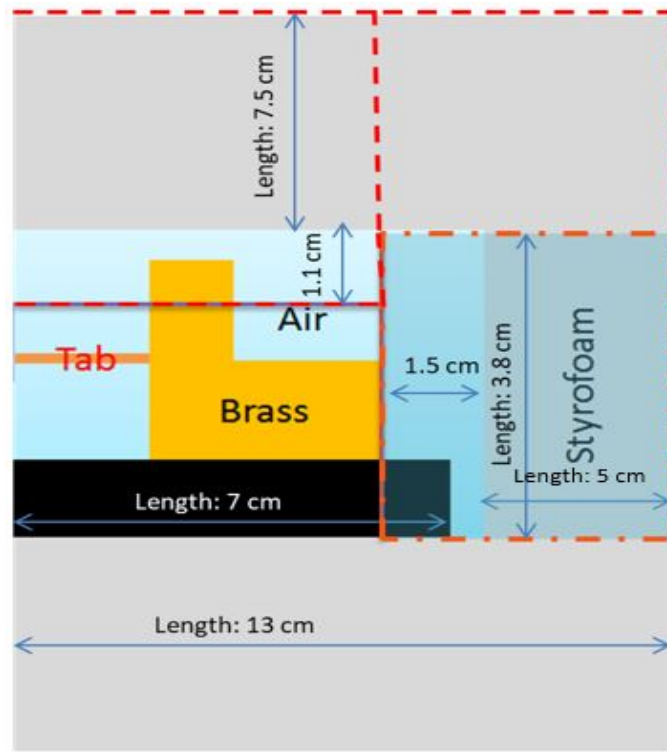


Figure 4.25: Single cell box setup

Table 4.8: Complex model: Resistane calculations for part-2

Components	Length <i>cm</i>	Breadth <i>cm</i>	Area <i>meters</i>	Thermal conductivity $W/(m.K)$	Height <i>cm</i>	Thermal resistance K/W
Brass top _x	7.2	1	0.00072	109	1.5	0.1911
Brass bottom*2 _x	9	1	0.0009	109	4.3	0.4383
Tab _x	0.2	2.7	0.000054	238	4.5	3.5014
Brass bottom*2 _y	9	4.3	0.00387	109	1	0.0237
Brass top _y	7.2	1.5	0.00108	109	1	0.08494
Air _y + Styrofoam _y	33	6.5	0.02145	0.0273	8.6	146.861
Styrofoam top	33	6.5	0.02145	0.033	7.5	105.954
Air _x + Styrofoam _x	20.9	3.8	0.00794	0.0286	6.5	286.165
Bakelite _y	20.9	7	0.0146	0.2	1.2	4.1011
Styrofoam bottom	13	40.6	0.0528	0.033	5	28.706

Similarly, K_{eff} for the box in red dotted line is $0.0273 W/(m.K)$. The thermal resistance for part 2 is calculated and shown in Table 4.8.

From Table 4.8, the thermal resistance of different components is taken and plotted into a network, as shown in Figure 4.26.

In Figure 4.26, only one tab and brass bar setup is considered. However, a combination of part-1 and part-2 is presented below in which both the positive, negative tabs and the brass bars are included. Figure 4.27 shows the combination of both

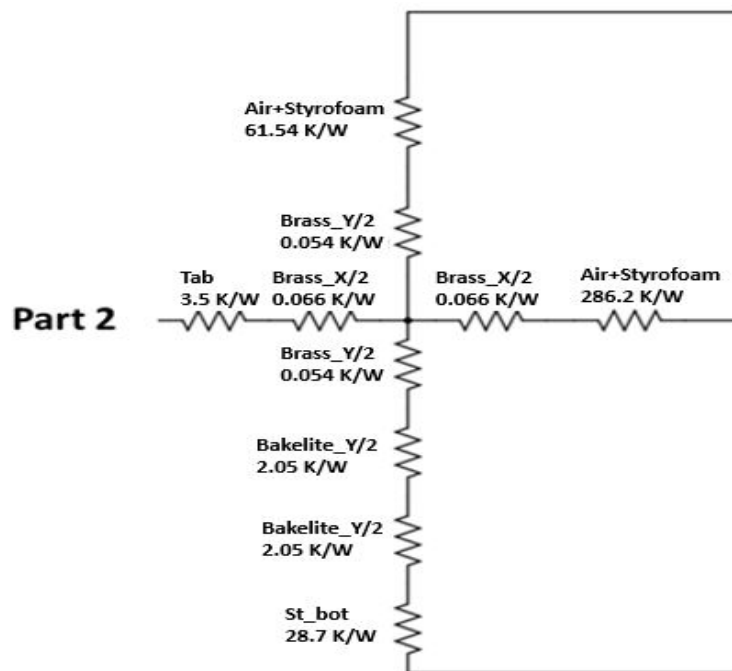


Figure 4.26: Complex model: Thermal resistance network Part-2

part 1 and part 2 of the thermal resistance network.

An LPN model considering resistance and capacitance for the entire complex box model is as shown in Figure 4.27. Here the thermal resistance of the top styrofoam block is estimated to be 25.5 K/W . However, this estimation did not take the heat spreading angle into consideration. So, the thermal resistance value is revised after considering the heat spreading angle, and the final version of the updated thermal resistance network is shown in Figure 4.28.

The thermal resistance network shown in Figure 4.28 fits better with both COMSOL and LPN models of the box setup. Hence a complex model of the box setup is needed for achieving a better match.

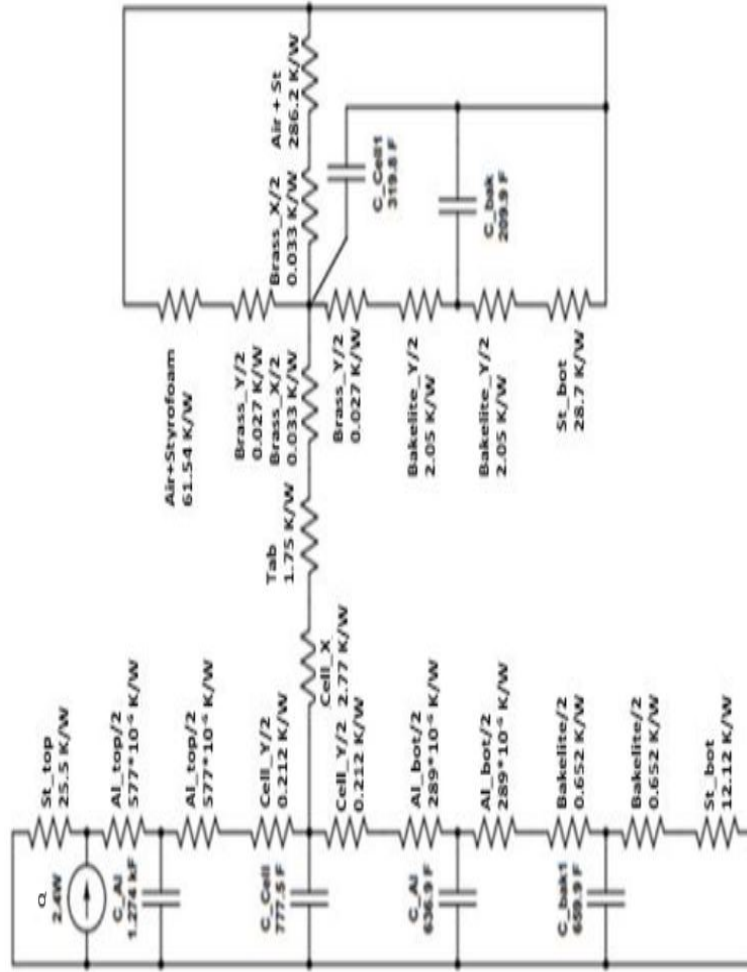


Figure 4.27: Thermal resistance network of the complete experiment setup

4.4 Box model with test setup and a cable attached

This section represents the actual physical model of the styrofoam box with a complete test set-up. Also, a cable is attached to one of the brass bars and the whole set-up is enclosed by styrofoam walls. Thus, this model is as a combination of sections 4.2 and 4.3. In the physical set-up, the cable end is transformed into a lug connector and then tightened to the brass bar through a screw. As this form of connection is hard to replicate in the COMSOL and LPN models, the most appropriate connecting means is selected through several adjustments. These adjustments are further described in 4.4.1. Both the COMSOL and LPN models of the model are presented below.

4.4.1 COMSOL Model

A COMSOL model for the test setup stated in section 4.3 along with the cable is modelled with the following considerations.

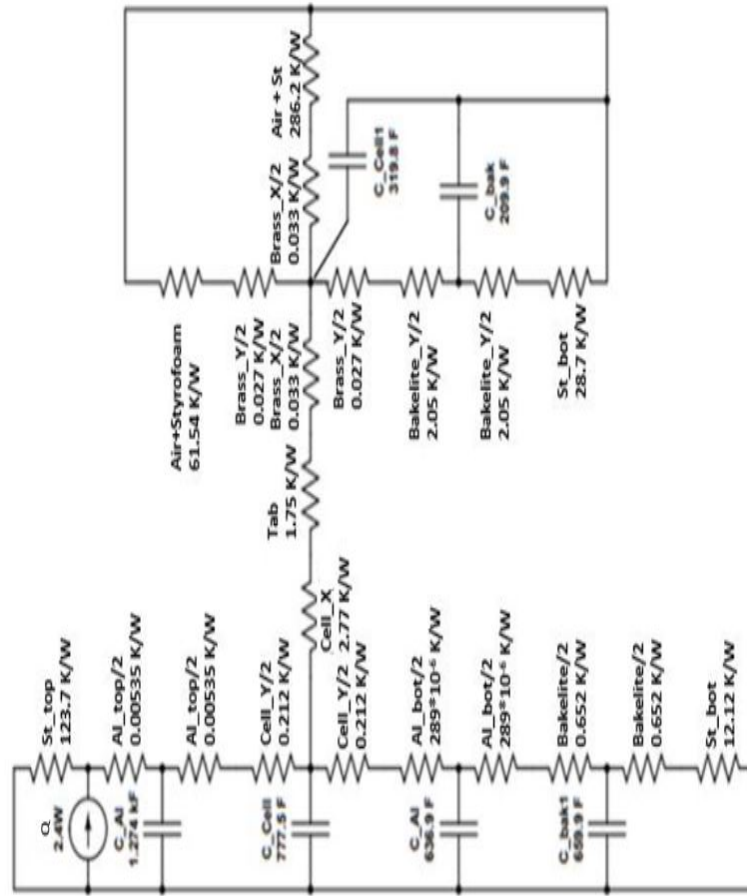


Figure 4.28: Updated thermal resistance network of complete experiment setup

Application mode: 3D, Heat transfer in solids (ht), Time dependent.

Geometry: All components of the enclosed test setup are created using 3D, as shown in Figure 4.29. In this model, a cable is attached to the sealed box setup. In the physical model, a cable lug and bolt are used to connect the cable to one of the brass bars. To replicate a similar connection between the cable and brass bar, different connecting blocks are tested and a square block, as shown in Figure 4.30 recreated the closest match to the physical model. All other blocks are modelled in the same way as shown in sections 4.2 and 4.3.

Materials: The material properties are the same as the materials selected in the case of Cable COMSOL model presented in section 4.2.1 and the Box model presented in section 4.3.2.1.

Physics: Under heat transfer in solids (ht), the temperature for the entire outer portion of the box is considered as 291.25 K . The heating mat is considered as a heat source and, a heat rate of 2.4 Watts is given as an input. The heat transfer coefficient at the outer surface of the cable is considered as $10\text{ W}/(\text{m}^2.\text{K})$.

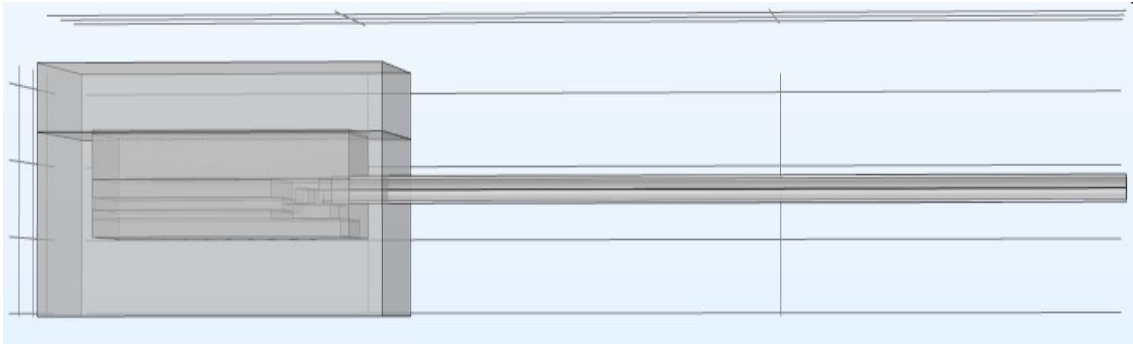


Figure 4.29: Battery box with cable: COMSOL model

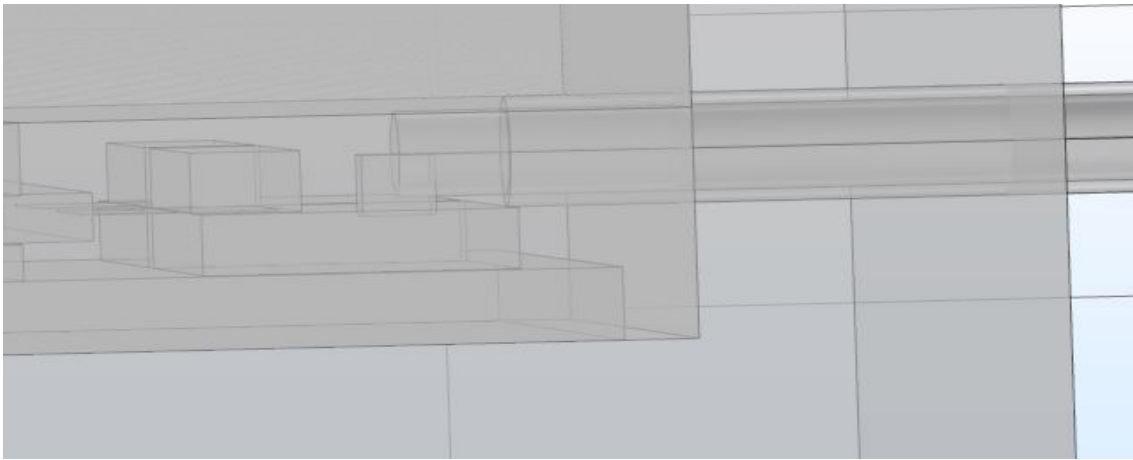


Figure 4.30: Battery box with cable: COMSOL model

Mesh: A fine mesh is selected from the physics-controlled mesh for all domains. The mesh parameters are,

- Number of elements: 90740
- Minimum element quality: 0.005512
- Average element quality: 0.5823
- Mesh volume: 0.0219 cubic meters

Study: A 'Stationary' study is used to understand the temperature dissipation through different components of the test setup.

Post processing:

- Six 'Cut point 3D' plots based on sensor location are created. These locations are on the aluminium plate, on the positive brass bar and on the positive tab.
- Six '1D point graphs' are created to analyze the temperature variations based on sensors location.

4.4.2 LPN Model

An LPN model for the experiment setup stated in section 4.3 along with the cable is modelled in this section. This LPN model is a combination of Figures 4.1 and 4.15.

The connection point is the same as the one described in the COMSOL model shown above. Also, the thermal resistance for the brass bar and the point at which the cable is connected to the brass bar is the same. This may result in no temperature variation at these points. Whereas in the physical model and COMSOL model, this will be different and a change in temperature variation can be observed.

The cable model presented in section 4.2.2, with the dimensions given in Table 4.1 is considered for modeling the cable LPN model and similarly the box model presented in section 4.3.2.4, with the dimensions given in Table 4.3 are considered for modeling the box LPN model.

Thus, both the models are created using appropriate equations as presented in sections 4.2.2 and 4.3.2.4. An LPN model of the combination is shown in Figure 4.31.

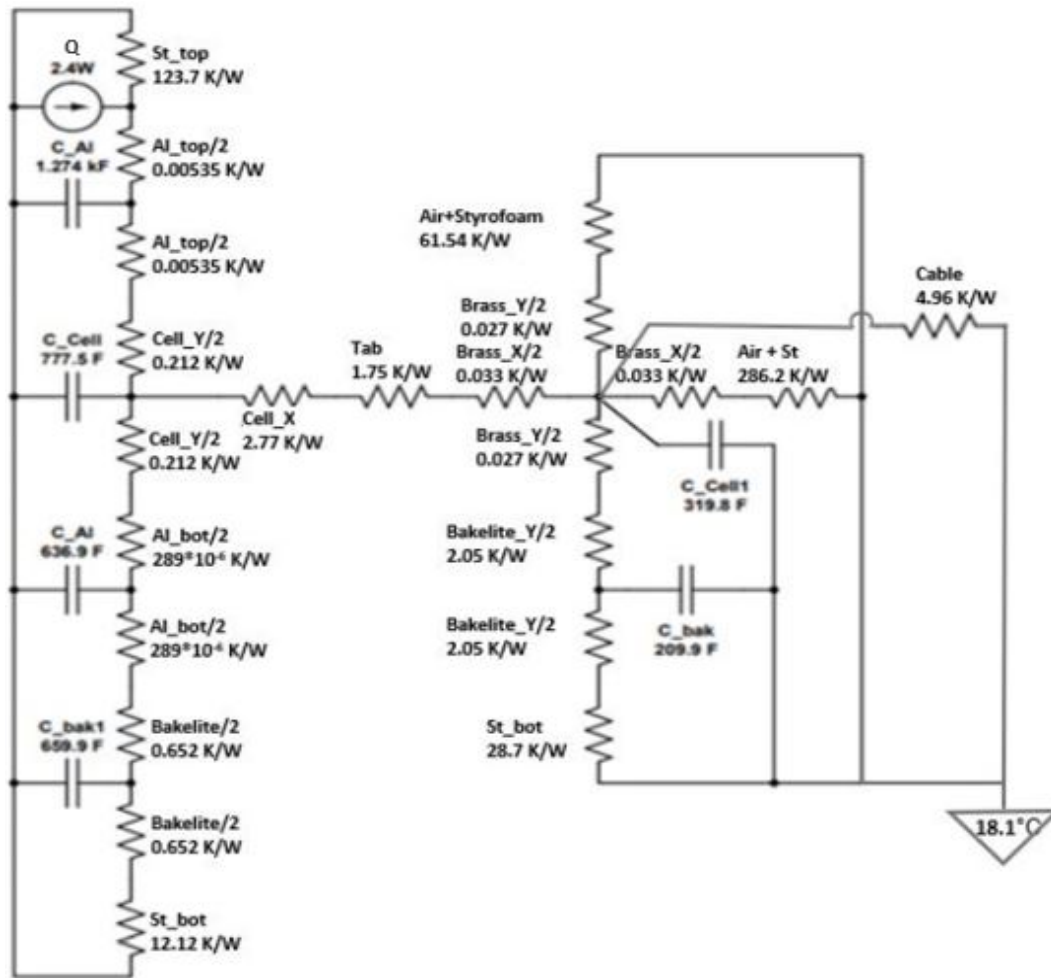


Figure 4.31: Box model with experiment setup and a cable attached

A comparison of the COMSOL model, the LPN model and a practical model of a 'Box with experiment setup and a cable attached' is presented in the next chapter.

5

Results

Results from the COMSOL model, the LPN model and the measurement data from the physical model are compiled. The results are analyzed and the information necessary to conclude is gathered from this section.

5.1 Single cable: comparison of LPN VS COMSOL

5.1.1 Results from the COMSOL model

Figure 5.1 illustrates the COMSOL model after post-processing along with considerations and dimensions stated in section 4.2.1. The temperature, in this case, is indicated in kelvins with a range of $292.15K$ to $296.15K$, which translates to $19^{\circ}C$ and $23^{\circ}C$.

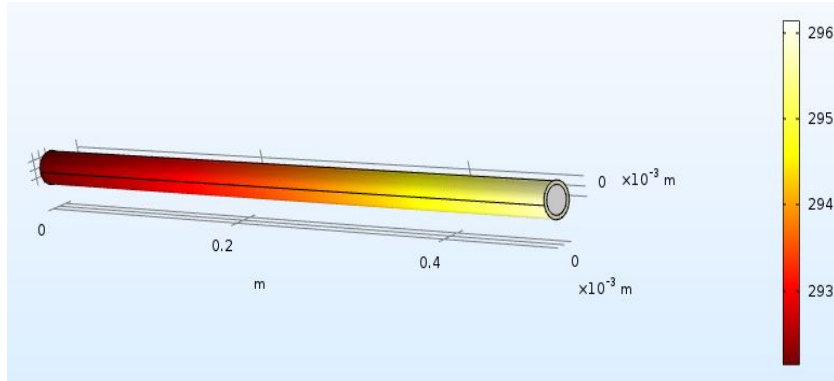


Figure 5.1: Temperature variation in the cable using the COMSOL model

The temperature difference along the cable at selected points as shown in Figure 4.3, are plotted in a chart and illustrated in Figure 5.3.

From Figure 5.3, it can be observed that the change in temperature along the cable is uniform for the selected convective heat transfer coefficient of $h = 10W/(m^2.K)$.

The results from this COMSOL model are compared to the LPN model presented

in the next section, and the temperature differences between these two models are discussed in detail.

5.1.2 Results from the LPN model

Figure 5.2 shows the LPN model presented in section 4.2.2, including the thermal resistance values at each 5 cm length segment and for a total cable length of 50 cm. The temperature differences along the length of the cable is shown in Figure 5.3, starting with 23°C at the length of 0 cm and ending with 19°C at 50 cm.

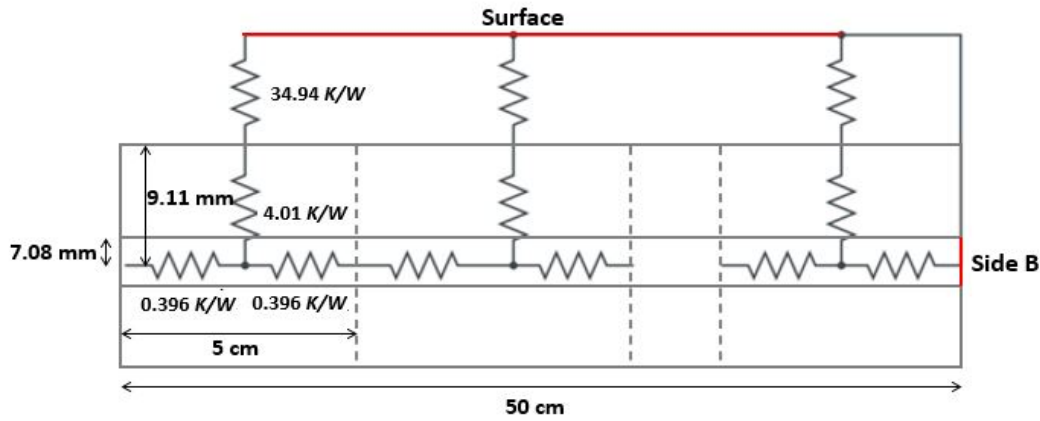


Figure 5.2: Cable: Thermal resistance network

The temperature distribution along the cable seems to be uniform, and these values are further compared with the temperature differences along the cable in the COMSOL model.

Results from both representations of the cable models, i.e. the COMSOL model and the LPN model are compared in Figure 5.3. From this figure, it can be observed that the temperature distribution in the cable along the length in COMSOL model and LPN models are in good agreement with each other.

As the temperature difference between these two models is low, both models are considered to be in good agreement with each other. Thus, the same approach is considered for the cable used in the box set up and cable set up used in the study.

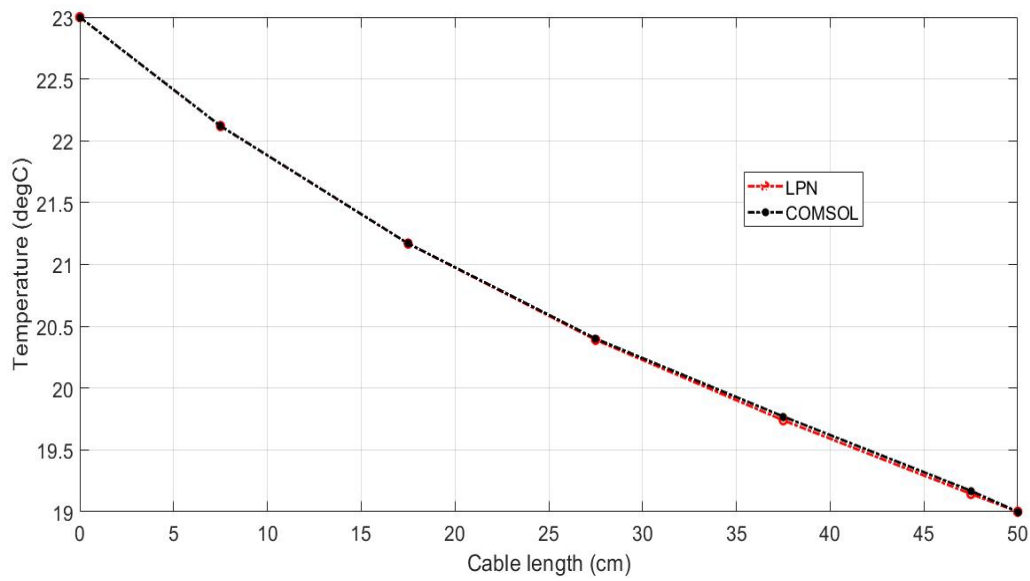


Figure 5.3: COMSOL vs LPN: Temperature variation along the cable

5.2 Box model: comparison of LPN VS COMSOL

5.2.1 Results from the COMSOL model

Figure 5.4 illustrates the COMSOL model after post-processing along with considerations and dimensions stated in section 4.3.1. The temperature difference along the box is indicated by the scale next to the model shown below, and the units are in degree centigrade.

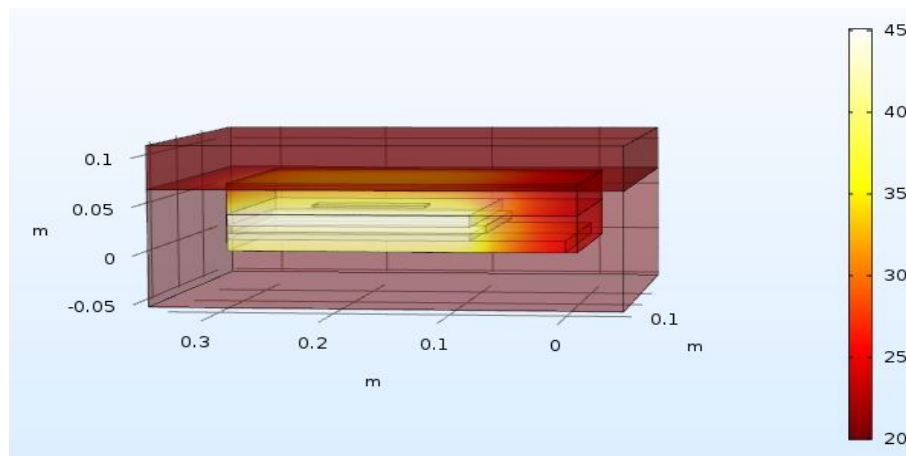


Figure 5.4: COMSOL model: Temperature variation in the box without complete test setup

The temperature difference along the box set up at different points is plotted and presented in Figure 5.6. From Figure 5.6, it is observed that the temperature difference between the node at the heating mat and the node at the cell is varying at the

same rate in comparison to the temperature difference between the node at the cell and the node located on the bottom aluminium plate. An increase in temperature difference between the points located on the bottom aluminium plate and styrofoam bottom is due to the higher thermal resistance of the bakelite plate.

5.2.2 Results from the LPN model

Considering the temperature at the point located on the heating mat as a reference, all temperature variations along different points are calculated and presented in Figure 5.5.

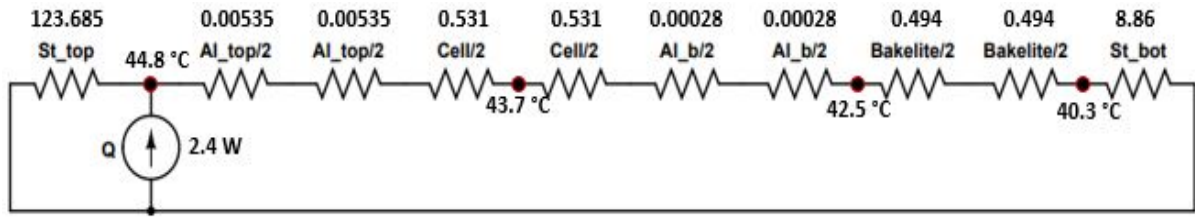


Figure 5.5: Thermal resistance network of box model without complete test setup

In this case, the temperature generated inside the box is less than that of the temperature generated in the COMSOL model. However, the difference in temperature seems to be uniform from the node point at the heating map to the point located on top of the bakelite plate. The temperature variations in the LPN model are shown in Figure 5.6.

5.2.3 Comparison between COMSOL and LPN models

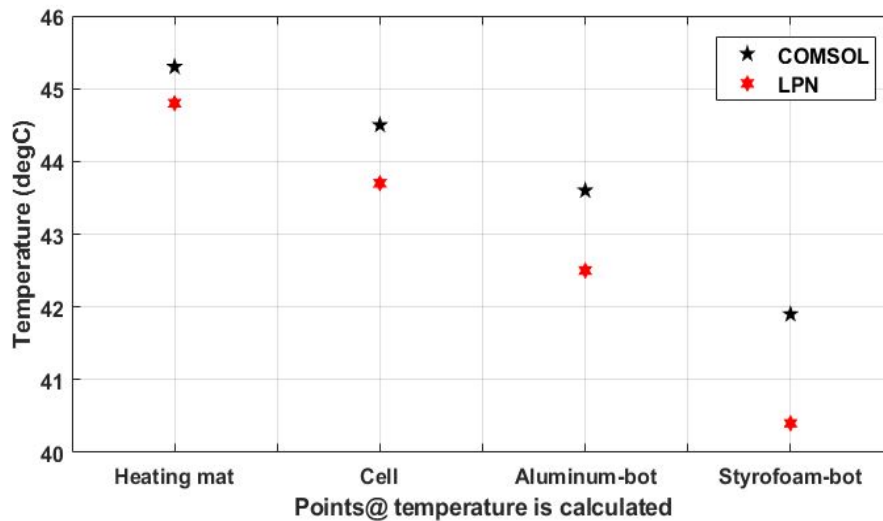


Figure 5.6: COMSOL vs LPN: Temperature measured at different locations

Results from both models are plotted in Figure 5.6. From this comparison, it is clear that the temperature difference between both models is minimum at the point

of the heat source and is increasing uniformly going further. However, the change in temperature from the point of the heat source to the point located at styrofoam bottom is similar in both models.

To understand the temperature change in both models, the thermal resistance of the styrofoam enclosure and the components in contact with air inside the box are studied more closely. A few factors affecting the change are described below.

- **Top styrofoam block:** In the LPN model, a heat spreading angle [16] is considered for the calculation of thermal resistance and the calculations, using a spreading angle constitute an error of up to 5% in general. The variation in thermal resistance calculated using the heat spreading angle could be one of the factors affecting the temperature difference in this case. However, this is the most relevant and simple means to measure the heat spread involving such components in an LPN model.
- **Air inside the box:** Air plays a major role in this case as it occupies a significant portion of the box. Apart from the air present in the X direction of the cell, the air is also present next to the aluminium and cell blocks. In the case of aluminium plates, this may be negligible, but for the cell, the presence of air covers approximately 3 *cm*, which could be an additional reason for the temperature difference. However, this difference is less in this particular case.
- **Bottom styrofoam block:** The assumptions related to the unfolding of the styrofoam block portion located on the side of the aluminium plates, the cell and consideration of an entire styrofoam bottom block for resistance calculation, increases the resistance value to a certain extent in an LPN model. After further observation considering the heat spreading angle, the thermal resistance in different blocks and selected materials, the best fit is used in the current LPN model.

Considering the components that have a major influence on temperature variation in the box setup, these cases are investigated further, and more precise evaluations are presented in section 4.3 of the test setup.

5.3 Single cell sealed box

5.3.1 Results from the COMSOL model

Fig. 5.7 presents the COMSOL model after post-processing along with considerations and dimensions stated in section 4.3.2.4. The temperature difference along the box is indicated by a scale next to the box model and units are in degree centigrade.

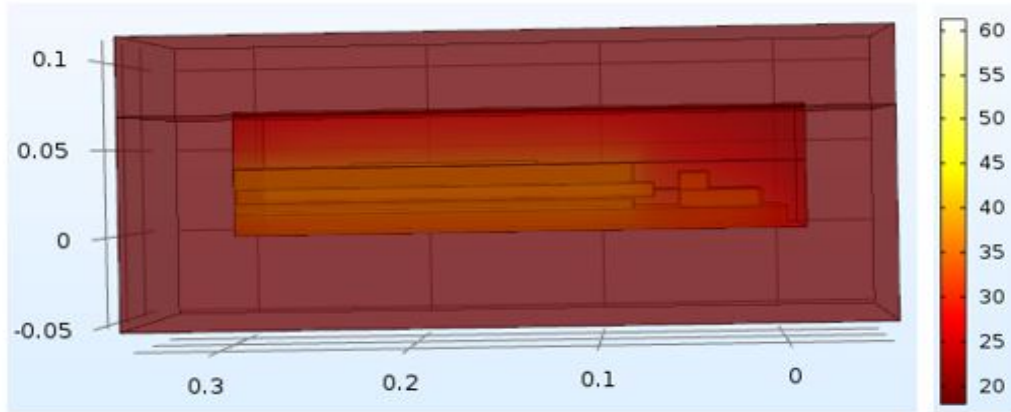


Figure 5.7: COMSOL model: Temperature variation in the box with the complete test setup

The temperature variation along the box set up at different points, as shown in Figure 4.14 are plotted and presented in Figure 5.9. From Figure 5.9, it is observed that the temperature change from the point located at aluminium plate on top of the cell to the point located at the cell block is at a uniform rate. However, there is a big change in temperature between the cell block and the tab. One of the reasons for such a temperature change is that the thermal conductivity values considered for cell block, as shown in Table 4.7, i.e. the thermal conductivity values for the cell are 29 W/(m.K) in the X direction and 0.5 W/(m.K) in the Y direction. These values are quite low in comparison to the thermal conductivity of aluminium. Also, due to the contact between the tab and the cell block, the amount of heat transfer is quite low and therefore, the temperature difference is higher.

The results from both the COMSOL and LPN models are compared to better understand the variations in temperature along the box.

5.3.2 Results from the LPN model

The temperature at the node point of the aluminium piece is considered as a reference point and temperatures at different locations, as shown in Figure 5.8 are calculated and presented.

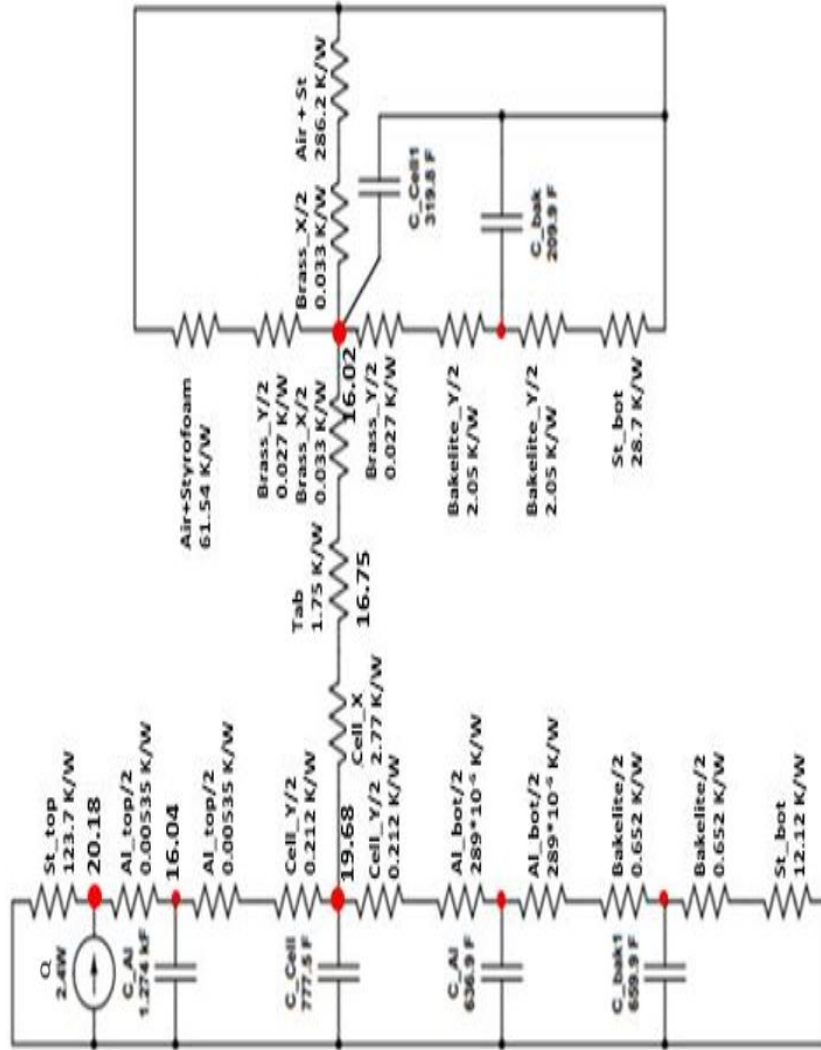


Figure 5.8: Thermal resistance network of box with complete test setup

The temperature generated inside the box, in this case, is less than that of the temperature generated in the COMSOL model. However, the temperature difference seems to be uniform from the node point at the aluminium piece till the point located on cell. The temperature variations from the LPN model are shown in Figure 5.9.

5.3.3 Comparison of COMSOL and LPN models

Results from both the LPN and COMSOL models along with the 'measured' values from the lab experiment setup of the practical model are plotted in Figure 5.9. From this comparison, it is clear that the temperature difference between both models is minimum at the point of the heat source and is increasing uniformly, going further. However, the difference in temperature at the cell and tab is higher in the case of LPN model than the COMSOL model.

Further, to understand the mismatch in both models at the cell and tab, a few components/ features that could have an impact are studied closely.

- **Top styrofoam block:** In the LPN model, heat spreading angle from section 2.7 is considered for the calculation of thermal resistance and the calculations, using a spreading angle constitute an error of up to 5% in general. The variation in thermal resistance calculated using a heat spreading angle could be one of the factors affecting the temperature difference at the source. From the source (i.e., aluminium top block), the temperature variation between the LPN and the COMSOL model are similar till the point at the Cell.
- **Air inside box enclosure:** Air plays a major role in this case as it occupies a significant portion of the box. Air is present on top of the test setup and in between the cell and the test setup. In addition to the air present in the X direction of the cell, the air is also present next to the aluminium and cell blocks. In the COMSOL model, the air inside the box gets heated and thereby affects the heat transfer rate from cell to the test setup. Whereas in an LPN model, only individual resistances of each block are considered. The thermal conduction in the air present between the cell and the test set up and the air present between the cell and styrofoam blocks is not considered. Therefore, this could be one of the reasons for a temperature difference of 1.3 degrees from the cell to the tab in the LPN model. From the point at the tab, the temperature change remains the same in both cases till the point at brass bar.

Temperature measurements from Figure 5.9 shows that the measurements from the practical model are in good agreement with the measurements from LPN model.

The difference between temperature measurements in the practical model and the COMSOL model indicates that there is a heat leakage while performing tests practically. Though cotton is placed in between the cell and brass bars in the experiment setup, heat leakage took place in the box while experimenting. In the next case, these temperature changes are further verified, when a cable is attached to the brass bar in a practical experiment setup. Temperature measurements from Figure 5.9, indicate that the measurements from the practical model are in good agreement with the measurements from the LPN model.

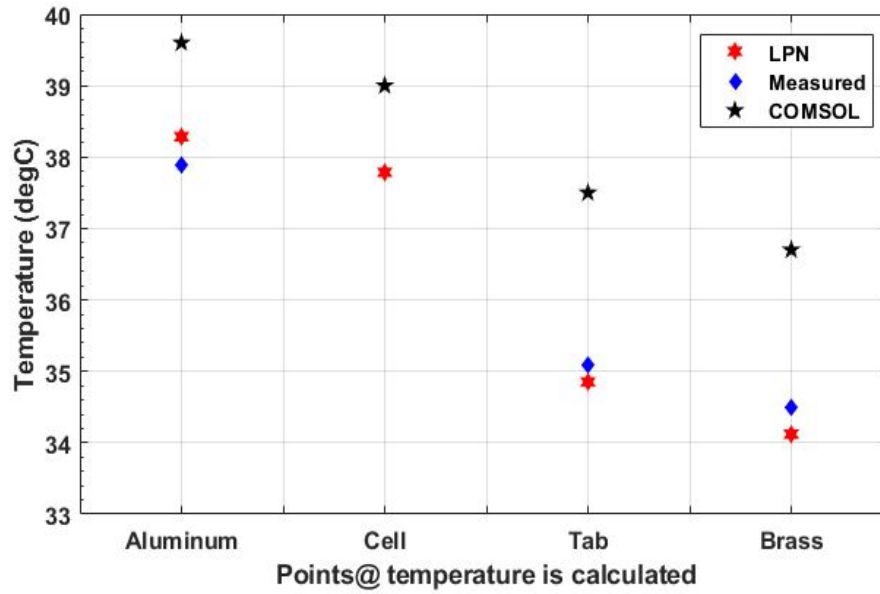


Figure 5.9: Temperature measurements comparison between COMSOL, LPN and Practical model

5.4 Box model with a cable attached

5.4.1 Results from the COMSOL model

Figure 5.10 illustrates the COMSOL model after post-processing along with considerations and dimensions stated in section 4.3.2.4. Temperature variation along the box is indicated by the scale next to the box model and units are in degree centigrade.

The difference in temperature along the box set up at different points is plotted and presented in Figure 5.12. From Figure 5.12, it can be observed that the temperature change from brass bars towards the end of the cable is uniform, indicating consistency in heat transfer rate. However, a drop in temperature can be observed from aluminium to tab, and same is valid for the case between the tab and brass bars. As discussed in the previous section, the low thermal conductivity of cell in the X direction, the tabs and heat loss along the cable could be the main factors affecting such a change.

The results from both the COMSOL model and LPN model are compared to better understand the variation in temperature along the box.

5.4.2 Results from the LPN model

The temperature at the node point of the heating mat is considered as the reference point, and the temperature change along different points is calculated and presented in Figure 5.11.

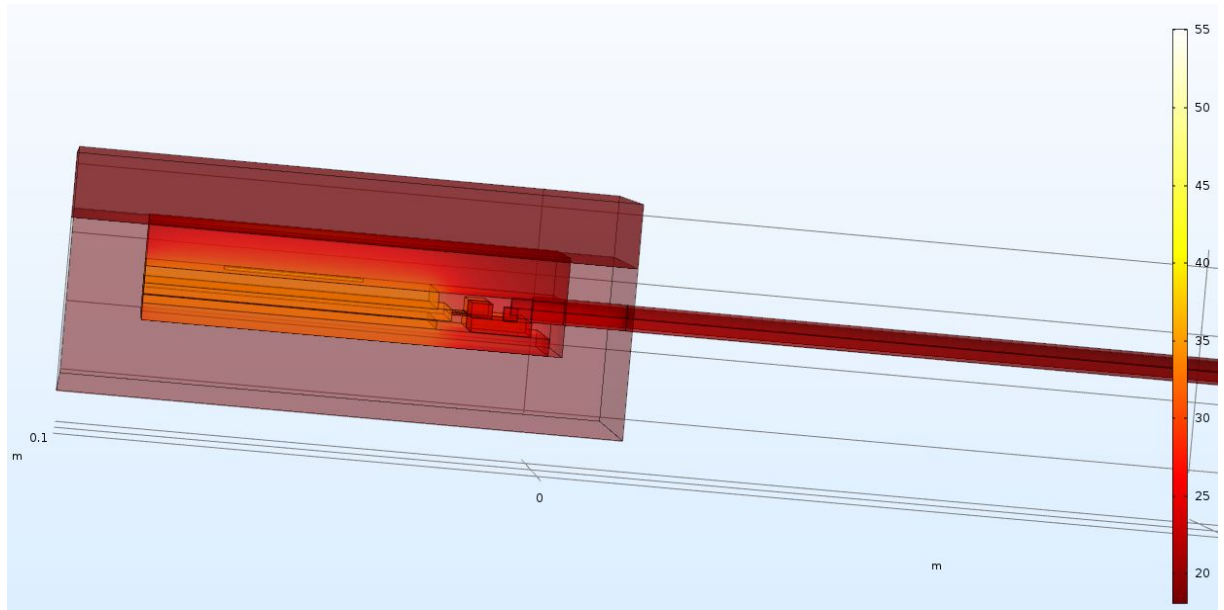


Figure 5.10: COMSOL model: Temperature variation in the box with a cable attached

In this case, the temperature generated inside the box is lower than that of the temperature generated in the COMSOL model. However, the temperature change seems to be uniform from the node point at the brass bars till the end of the cable. Also, the temperature at the brass bars and the connecting point of cable are the same due to the consideration of same thermal resistance in both cases as described in section 4.4.2.

The temperature variations from the LPN model are shown in Figure 5.12.

5.4.3 Comparison of COMSOL and LPN models

The results from all the models are plotted in Figure 5.12. From this comparison, it is clear that the temperature variation in all the three models from the point at the brass bars till the end of the cable is uniform. However, the temperature from the point at aluminium to the point at brass bars is not changing at a uniform rate in all models. The factors affecting this change are discussed below.

- **Thermal conductivity in cell and tab:** In both the COMSOL and the practical models, heat is transferred from the cell to the brass bars through the tabs located in between. The thermal resistance in the direction of the heat flow from the cell to the brass bars is higher in comparison to the thermal resistance in other components.
- **Air inside the box:** Air occupies a significant portion in the box. In the

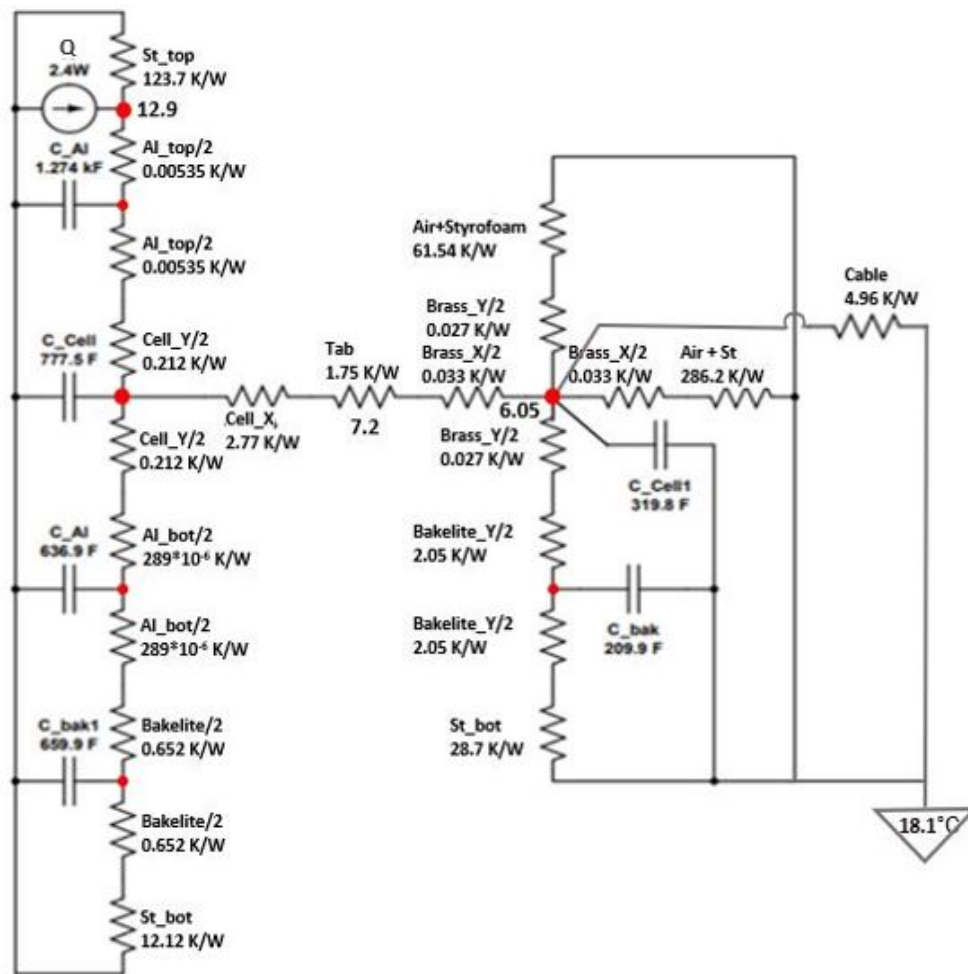


Figure 5.11: Thermal resistance network of the complete experiment setup

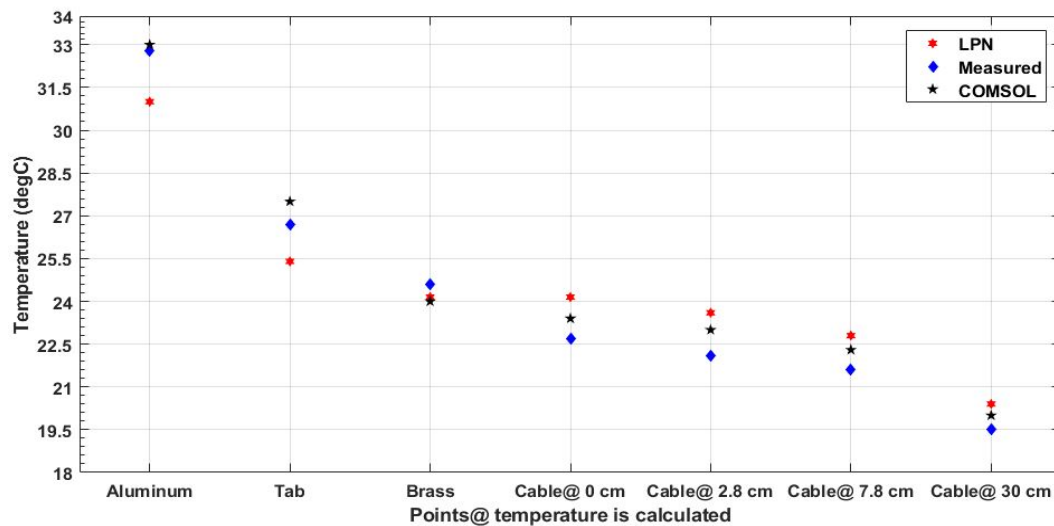


Figure 5.12: Comparison of measured temperatures in LPN, COMSOL and Practical models

COMSOL model, the experiment setup is enclosed by a styrofoam box, thus there is no heat leakage. In a practical experiment setup, cotton is placed around tabs and on top of brass bars to prevent heat leakage and provide better insulation. However, it seems that there is still heat loss in the practical experiment setup and from Figure 5.12, it can be observed that this heat loss is quite low and both models are in good agreement.

In the LPN model, conduction through the air around the aluminium plates, the cell and the tabs is not taken into account. In addition to the cable connection structure, this seems to affect the temperature variation at the tab in both the models.

- **Styrofoam block:** In the LPN model, a heat spreading angle is considered for the calculation of thermal resistance and calculations using the spreading angle constitute an error of up to 5% in general. The variation in thermal resistance calculated using the heat spreading angle could be one of the factors affecting temperature difference at the aluminium block.

Though temperature variations are different in all the three models at the aluminium block and the tab, results from the COMSOL model and the practical experiment model are in good agreement with each other.

5.5 Temperature variation at different heat rates

In all the earlier sections the applied heat rate is $2.4W$. In this case, the box model with test setup presented in section 4.3.2.4, is taken as reference and the temperature at different sensor locations is noted at different heat rates, i.e. $1W$, $2.4W$, $3W$ and $4W$. Similarly, for different heat rates the temperatures at different node points are calculated in corresponding LPN models.

The temperature values from both the COMSOL and LPN models, when different heat rates are applied are presented in Table 5.1.

From Table 5.1, the temperature difference in both models in the case of Aluminum, Tab and Brass bars is changing at a uniform rate.

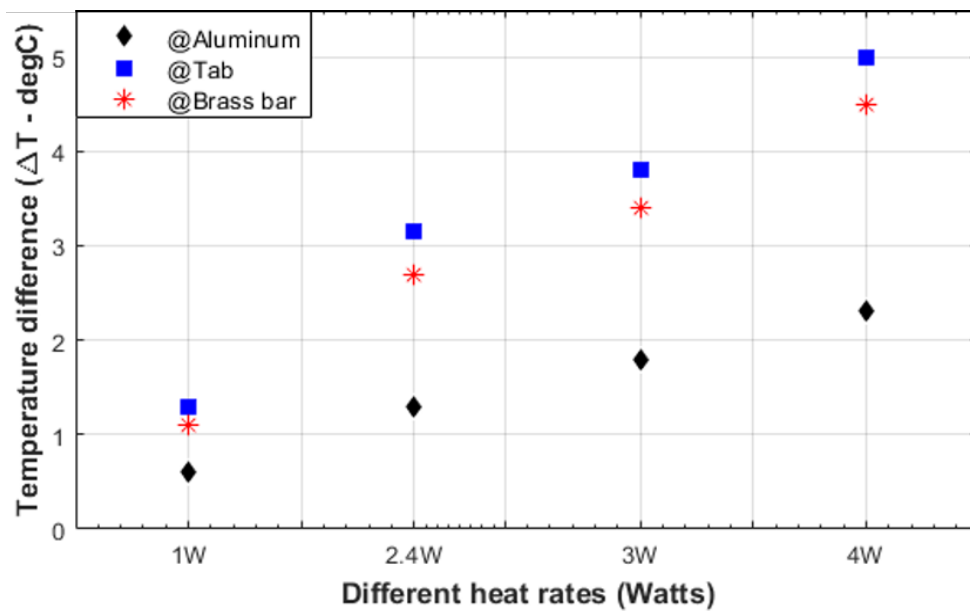
The difference in temperatures at the same location in both the models is compared and presented in Figure 5.13. From Figure 5.13, it can be understood that the temperature variation is at a uniform rate with a uniform increase for the heat rate applied.

From Table 5.1, the temperature difference in both models in the case of points Aluminum, Tab and Brass bars is changing at a uniform rate. Thus, from these

Table 5.1: Temperature distribution in the box model with test setup at different heat rates

Different heat rates		1W	2.4W	3W	4W
COMSOL	Aluminum (in °C)	27.1	39.6	45.1	54
	Tab (in °C)	26.35	38	42.8	51
	Brass bar (in °C)	25.9	36.8	41.5	49.3
LPN	Aluminum (in °C)	26.5	38.3	43.3	51.7
	Tab (in °C)	25	34.85	39	46
	Brass bar (in °C)	24.8	34.1	38.1	44.8

comparisons, it is observed that the resulting box model compare well in both the COMSOL and LPN models. Thus, despite some temperature differences, the resulting LPN model closely resembles the COMSOL model.

**Figure 5.13:** Temperature difference between the LPN and COMSOL models at different heat rates

5.6 Temperature variation in the Box model with cable attached and assuming air flow

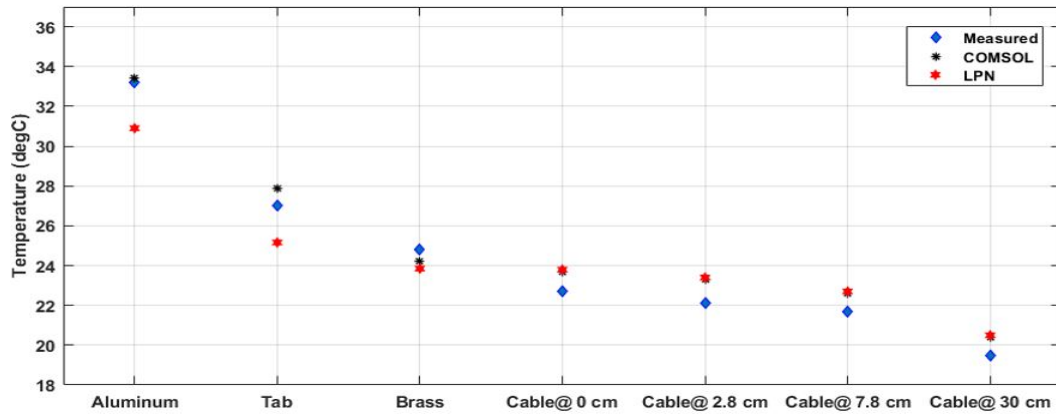
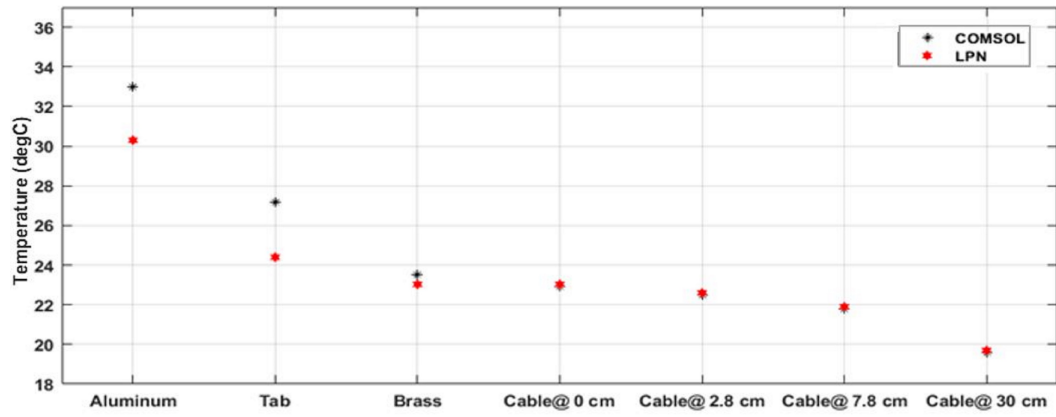
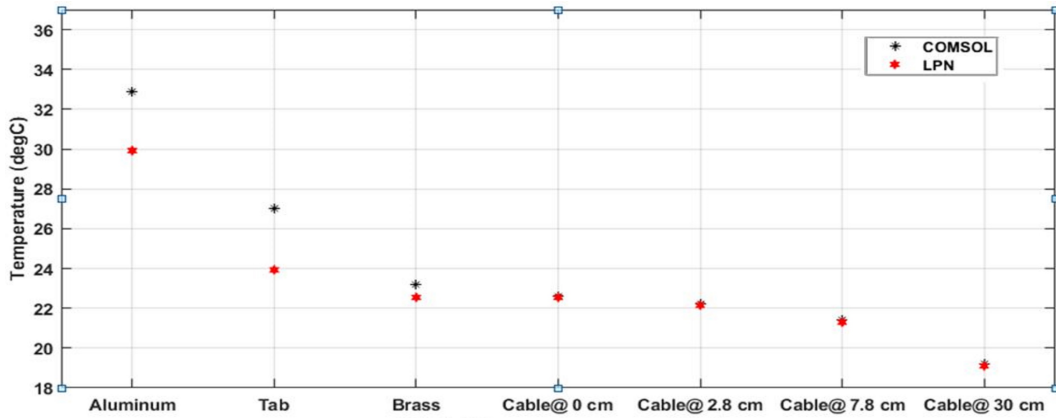
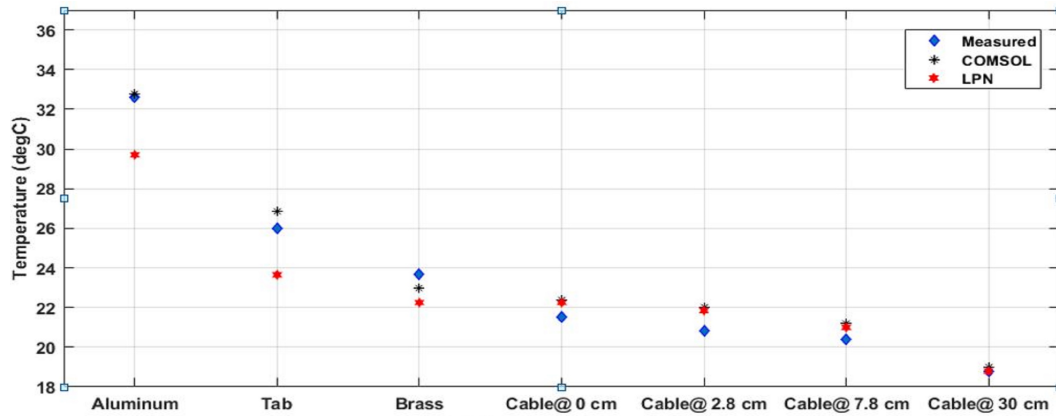
The comparison between COMSOL and LPN model presented in section 5.4 is performed assuming no airflow outside the box. Though the test setup surrounded by thick styrofoam walls does not get affected due to a change in airflow outside the box, the cable attached to the box model will have a significant temperature change due to a change in airflow. Therefore, in this section, the thermal convection coefficient h along the cable is varied, and the temperature change in the box model is presented.

Figures 5.14 to 5.17 illustrates the comparison between COMSOL and LPN models when the thermal convection coefficient h surrounding the cable is in the range of 10 to 40 $W/(m^2.K)$.

From Figures 5.14 to 5.17, it can be observed that there is a change in temperature with a change in air flow rate around the cable. Also, the temperature change is not significant when the thermal convection coefficient is changed from 30 to 40 $W/(m^2.K)$.

In all cases, the temperature change between COMSOL and LPN models are in good agreement. However, the difference in temperature change at aluminum and tab is high in comparison to the points at the brass bar and along the cable. The factors contributing to such a difference is presented in section 5.4.

Though the temperature change inside the the box is different in COMSOL and LPN models, the temperature variations are uniform with the change in air flow rate along the cable and the same can be observed in Figures 5.14 to 5.17.

Figure 5.14: Cable with $\alpha=10W/(m^2.K)$ Figure 5.15: Cable with $\alpha = 20W/(m^2.K)$ Figure 5.16: Cable with $\alpha = 30W/(m^2.K)$ Figure 5.17: Cable with $\alpha = 40W/(m^2.K)$

6

Conclusion

From the information available in the result section, conclusions on the resulting LPN model are drawn and presented in this section. The scope and extent of the conclusions can be further discussed

6.1 Conclusions

The presence of air and thermal conductivity of the tab plays a major role in the temperature variation between the thermal and the LPN models. Yet, these variations are uniform with a change in applied heat rate and the resulting LPN model is in good agreement with the thermal model. Temperatures at all the node points located on each component of the test setup can be calculated using this simplified LPN model.

Given, the differences between the thermal model and the practical test setup, i.e. the heat leakage through the air in the practical test setup and the thermal model without any heat leakage; the lug structure for connecting cable in the practical test setup and usage of a cube block for the same in thermal model, the temperature difference exist. The presence of air inside the box is one of the main factors affecting these variations. However, in the resulted LPN model, these differences are monitored closely except for the connection structure in between cable and box model. The comparison of the LPN and thermal models at different heat rates confirm the same with a uniform change in temperature along with different locations. Thus, affirming the closeness of this LPN model to the thermal model at different heat rates. Therefore, this model can be applicable in cases, where an accurate thermal model can be modelled from a practical experiment setup.

To further evaluate real-life scenarios the box can be connected with two cables and temperature variation in the box, can be observed with and without an airflow outside the box. Also, a mathematical model incorporating the uniform change rate between the thermal and LPN models can be created to increase the closeness between these two models.

Bibliography

- [1] Marcy Lowe, Saori Tokuoka, Tali Trigg and Gary Gereffi. "Lithium-ion Batteries for Electric Vehicles: THE U.S. VALUE CHAIN" (2010).
- [2] Incropera, Frank and David DeWitt. "Introduction to heat transfer." (1985).
- [3] Incropera, Frank; David DeWitt; Bergman, Theodore and Lavine, Adrienne. "Fundamentals of Heat and Mass Transfer (6th ed.)" (2010).
- [4] "License Agreement for the Manufacturing and Sales of Electrolyte Material for Lithium Ion Batteries". Hitachi Chemical Co., Ltd. (2018).
- [5] Feng Leng, Cher Ming Tan and Michael Pecht. "Effect of Temperature on the Aging rate of Li Ion Battery Operating above Room Temperature". (2015).
- [6] Electropedia: "Battery Life (and Death)"
<https://www.mpoweruk.com/life.html>
- [7] Jang Wook Choi and Doron Aurbach. "Promise and reality of post-lithium-ion batteries with high energy densities". Nature Reviews Materials volume 1, (2016)
- [8] "Types of battery cells"
[https://batteryuniversity.com/index.php/learn/article/type of battery cells](https://batteryuniversity.com/index.php/learn/article/type%20of%20battery%20cells)
- [9] "PRISMATIC POUCH BATTERY PACKS"
<https://www.epectec.com/batteries/prismatic-pouch-packs.html>
- [10] "Thermal conductivity of common materials"
<https://www.engineeringtoolbox.com/thermal-conductivity-d-429.html>
- [11] <https://www.mplso2.com/assets/downloads/ELE-2501.pdf>
- [12] "American wire gauge"
[https://en.wikipedia.org/wiki/American-wire-gauge](https://en.wikipedia.org/wiki/American_wire_gauge)
- [13] <https://www.makeitfrom.com/material-properties/EPDM>
- [14] F.N. Masana. "A closed form solution of junction to substrate thermal resistance in semiconductor chips". IEEE (1996).
- [15] R. David. "Computerized Thermal Analysis of Hybrid Circuits". IEEE (1977).
- [16] Rick L. Sturdivant, Astacian J. Bogdon, Edwin K. P. Chong. "A Simple Closed Form Solution to Single Layer Heat Spreading Angle Appropriate for Microwave Hybrid Modules". Scientific Research Publishing Inc (2016).
- [17] Anton Lidbeck and Kazim Raza Syed. "Experimental Characterization of Li-ion Battery cells for Thermal Management in Heavy Duty Hybrid Applications". Department of Energy and Environment - Division of Electric Power Engineering, CHALMERS UNIVERSITY OF TECHNOLOGY (2017).

A

Appendix 1

A.1 Others

The voltages at each capacitance is calculated by identifying the temperature drop at each resistance. Thus, the network can be shown as

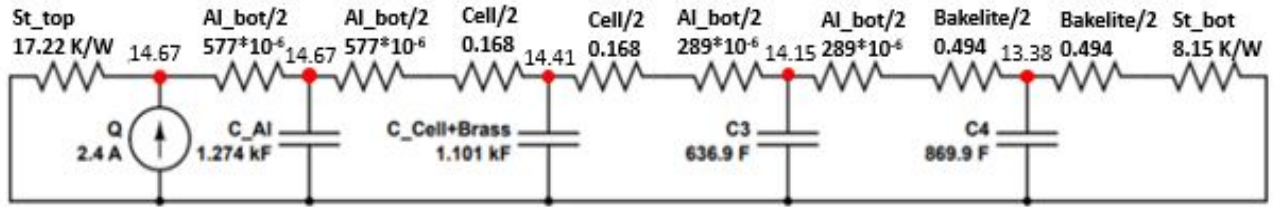


Figure A.1: Simple model: LPN circuit with temperature at different locations

The column ‘Arrangement’ indicates the arrangement of different components and the calculation of the effective thermal resistance from the arrangement, taken from the Figure 10b.

The Temperature (voltage in the above network) at each node indicate, the maximum temperature capacity of each component in the circuit.

Using nodal analysis at the nodes indicated in ‘red’ and with numbers 1, 2 , 3, the voltage can be calculated as follows

When the capacitor is not at all charged, i.e., at time $t = 0$

$$\text{At node 1 } 4.729v_1 - 4.69v_2 = 2.4$$

$$\text{At node 2 } 4.982v_2 - 4.69v_1 - 0.2195v_3 = 0$$

$$\text{At node 3 } 0.2696v_3 - 0.2195v_2 = 0$$

There fore $v_1 = 16.04$, $v_2 = 15.66$ and $v_3 = 12.75$, which represent the temperature at each node as shown in the LPN model.

The voltages at each capacitance is calculated by identifying the temperature drop at each resistance. Thus, the network can be shown as

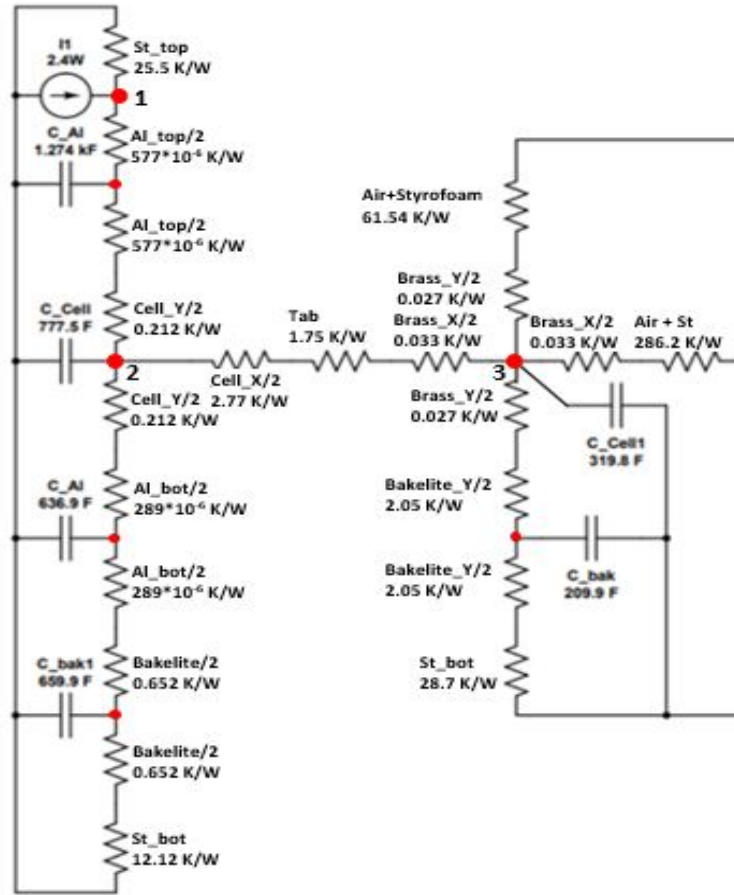


Figure A.2: Complex model: Resistance network of the combination: Part 1;
Part 2

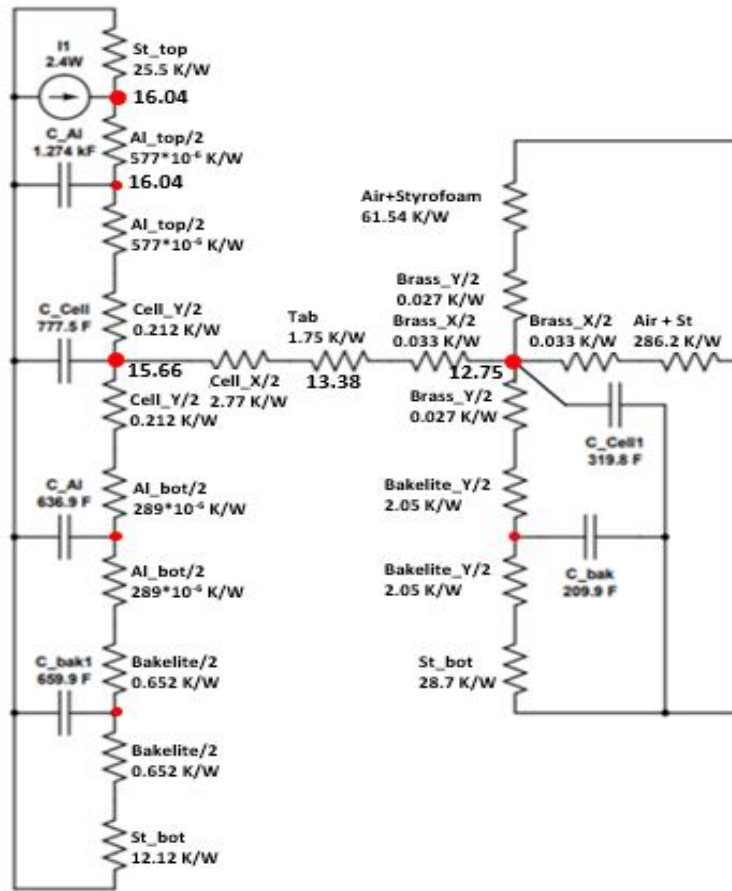


Figure A.3: Single cell box setup

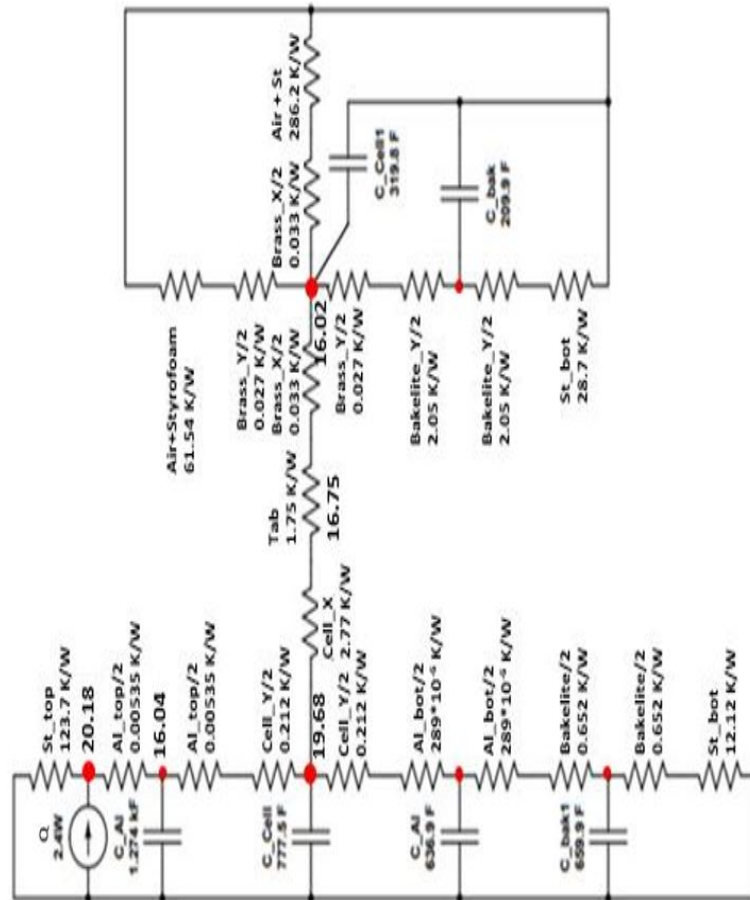


Figure A.4: Single cell box setup